THE JOURNAL OF PHYSICAL CHEMISTRY C

C: Surfaces, Interfaces, Porous Materials, and Catalysis

Organic Guests Within a Ferroelastic Host: The Case of High Silica Zeolite ZSM-5

Matteo Ardit, Annalisa Martucci, Luisa Pasti, Elisa Rodeghero, Giada Beltrami, and Giuseppe Cruciani

J. Phys. Chem. C, **Just Accepted Manuscript** • DOI: 10.1021/acs.jpcc.8b00686 • Publication Date (Web): 12 Mar 2018

ACS Publications

is published by the American Chemical Society. 1155 Sixteenth Street N.W., Washington, DC 20036

Organic Guests Within a Ferroelastic Host: The Case of High Silica Zeolite ZSM-5

Matteo Ardit,[1,*] Annalisa Martucci,[1] Luisa Pasti,[2] Elisa Rodeghero,[1] Giada Beltrami,[1] Giuseppe Cruciani[1]

[1]Department of Physics and Earth Sciences, University of Ferrara, Via Saragat 1, I-44122 Ferrara, Italy.
[2]Department of Chemistry and Pharmaceutical Sciences, University of Ferrara, Via Borsari 46, I-44123 Ferrara, Italy

[*]corresponding author e-mail: rdtmtt@unife.it

ABSTRACT

The physical-chemical properties of guest molecules confined within a zeolite framework host are known to be strongly affected by the confinement effects exerted through non-covalent host-guest interactions. Based on synchrotron time-resolved powder diffraction measurements and the Landau theory of ferroelastic phase transitions, we provide in this work evidence for the strong coupling existing between the thermodynamic properties of organic molecules (toluene, 1,2-dichloroethane, methyl-tert-buthyl-ether) adsorbed within the ZSM-5 zeolite and the lattice strain driving the monoclinic-to-orthorhombic (ferroelastic-to-paraelastic) phase transition which controls connectivity and diffusivity in the zeolite framework.

INTRODUCTION

High surface area, shape selectivity, mechanical, thermal, biological and chemical stability make ZSM-5 one of the most employed synthetic zeolites in adsorption processes of organic contaminants for wastewater treatments. In particular, ZSM-5 turns out to well succeed in the removal of toluene (TOL), 1,2-dichloroethane (DCE) and methyl-tert-buthyl-ether (MTBE) from waters, both as unary and binary mixtures.[1-5] The ZSM-5 zeolite (MFI framework topology) belongs to the pentasil zeolite family and it is characterized by a 3-dimensional pore system formed by two intersecting sets of tubular channels: the so called straight channel parallel to the [010] direction, and the sinusoidal channel parallel to the [100] direction.[6,7] Those channels have opening defined by 10 membered-rings (MR) of TO_4 tetrahedra with a free diameter which ranges from 5.4 to 5.6 Å and from 5.1 to 5.5 Å for the straight and the sinusoidal channel, respectively.

In the as-synthesized form, i.e. that obtained in alkaline medium and in the presence of tetrapropylammonium (TPA) template molecules, the topological symmetry of the ZSM-5 zeolite is orthorhombic (s.g. *Pnma*) with 12 independent T-sites in the unit cell. After thermal treatment the crystal symmetry is lowered to the monoclinic $P2_1/n$.[8,9]

Depending on composition,[7-18] framework defect density,[19] temperature,[10,20-24] or amount of guest compounds and nature of host-guest interactions within the channels,[8,25-33] synthetic ZSM-5 zeolite undergoes a polymorphic monoclinic ($P2_1/n$) to orthorhombic (*Pnma*, $Pn2_1a$, or $P2_12_12_1$) displacive phase transition.

Previously identified as a mutual shift of successive (010) pentasil layers along the *c*-axis,[20] X-ray single crystal experiments revealed that this phase transition involves a complicated displacement of framework atoms.[9-12] In detail, such a displacement is accompanied by changes in the population of single-crystal twin domains: i.e., aggregates of monoclinic twin domains change into an orthorhombic single crystal on increasing temperature.[9-12] Based on these evidences, it has been

suggested that the ZSM-5 monoclinic sample has the features of a ferroelastic material.[11,12,24] Nevertheless, through observations by coherent X-ray diffraction imaging it has been reported that, at local scale, traces of lattice strain can persist within the stability field of the orthorhombic paraelastic phase.[34]

In parallel to X-ray diffraction investigations, calorimetric analysis were performed to quantify the enthalpy variation associated with the monoclinic-orthorhombic ($m \leftrightarrow o$) phase transition. Besides to further highlight that the $m \leftrightarrow o$ phase transition has a displacive nature (i.e., subtle and reversible, with a same amount of enthalpy change involved in both heating and cooling processes)[18], these calorimetric investigations –carried out in Ar atmosphere after samples dehydration– rule out the possibility of co-adsorbed H_2O molecules involvement during the $m \leftrightarrow o$ structural rearrangement.[18,22,35]

In addition, it is well known that the aluminum content (i.e., Si/Al ratio) has a strong influence on both temperature of transition (T_c) and enthalpy change (ΔH) during the $m \leftrightarrow o$ phase transition of ZSM-5 zeolite compounds. Hence, the chemistry of ZSM-5 zeolite is intrinsically related with the thermodynamic of the $m \leftrightarrow o$ phase transition. Specifically, it has been pointed out that both T_c as well as ΔH define a curve with an exponential trend subordinated to the Al content, *i.e.*, the higher the Si/Al ratio, the greater both T_c and ΔH (silicalite samples with Si/Al > 5000 undergo $m \leftrightarrow o$ phase transitions that are usually characterized by $T_c > 350$ K and $\Delta H > 15$ kJ·mol^{-1}, whereas unloaded samples of ZSM-5 zeolite with a Si/Al < 1000 usually undergo $m \leftrightarrow o$ phase transitions at $T_c < 350$ K and $\Delta H < 15$ kJ·mol^{-1}).[18,24]

According to the Landau theory, the temperature-dependence evolution of an unloaded sample of highly siliceous ZSM-5 zeolite has been recently characterized and formalized through the analysis of the spontaneous strain variation revealing that the $m \leftrightarrow o$ phase transition has a tricritical character.[18]

Although numerous works deal with the thermodynamic features of the $m \leftrightarrow o$ ZSM-5 phase transition, the increasing interest in the scientific community on this compound employed as efficient adsorbent for the removal of organic contaminants from waters perfectly matches with the lack of information on the thermodynamic processes operating when organic contaminants are adsorbed within the ZSM-5 zeolite structure.

In this contribution, *in situ* high-temperature synchrotron X-ray powder diffraction data associated with gas chromatography and thermal analysis have been used to model the ferroelastic properties of the $m \leftrightarrow o$ phase transition of ZSM-5 zeolite samples loaded with organic contaminants as toluene (TOL), 1,2-dichloroethane (DCE), methyl-tert-buthyl-ether (MTBE), and a binary mixtures of them. Besides to provide further indications on the $m \leftrightarrow o$ phase transition, this investigation will shed light on the effects of organic molecules within the zeolite channels which affect the mechanisms of lattice strain, with particular emphasis at the occurrence of host-guest and guest-guest interactions.

EXPERIMENTAL SECTION

Sample description. Toluene, 1,2 dichloroethane, and methyl-tert-butyl-ether were purchased as analytical standards from Sigma-Aldrich with a purity of 99.8%, ultrahigh quality water, 18.2 MΩ cm, 0.22 μm filtered was obtained by Milli-Q® water purification system (Merk Millipore). High-silica ZSM-5 hydrophobic zeolite was provided by Zeolyst International (code CBV 28014) in its ammonium form and used as received. Electron micrographs of the ZSM-5 zeolite sample before organic molecules loading revealed that the investigated sample is composed of regular spherical particles, with diameters in the 2-4 μm range. Particle size distribution is uniform with a crystalline appearance.[36] The manufacturer of the CBV 28014 zeolite reports a SiO_2/Al_2O_3 molar ratio equal to 280, a Na_2O content lower than 0.05 wt.% and a surface area of 400 m^{2}g^{-1}. Each sample has been labelled according to the molecule or mixture of molecules loaded (*i.e.*, ZSM-5 loaded with toluene, TOL, toluene and 1,2 dichloroethane, TOL-DCE 1,2 dichloroethane, DCE, toluene and methyl-tert-

butyl-ether, TOL-MTBE, 1,2 dichloroethane and methyl-tert-butyl-ether DCE-MTBE, and methyl-tert-butyl-ether, MTBE).

Thermal analysis. Thermogravimetric (TG) and derivative thermogravimetry (DTG) measurements of ZSM-5 loaded with organic compounds were performed in air using an STA 409 PC LUXX®-Netzsch operating at 10 K min^{-1} heating rate, from room temperature (*RT*) to 1173 K.

XRPD at high-temperature: data collection. All data collections were carried out *in situ* at the ID22 high resolution powder diffraction beamline (European Synchrotron Radiation Facility, ESRF, Grenoble, France). Schematically, each sample was placed into a spinning capillary which rotated along the axis of the diffractometer. Once diffracted, the highly energetic incident X-ray beam (λ = 0.400031 Å) was directed through nine Si 111 analyzer crystals. Scanned in a continuous mode, nine high-resolution diffraction patterns were collected in parallel by means of nine scintillation detectors. Those registered patterns were normalized and combined in a subsequent data-reduction step to produce the equivalent step scan. X-ray diffraction patterns were recorded from room to a maximum temperature of 498 K (i.e., every 10 K up to 373 K and every 25 K for higher temperatures) in air, in the 0.5–19.5 2θ range.

XRPD refinement strategy. Unit-cell parameters were determined from whole pattern profile fitting of the diffraction data in a sequential mode through SEQGSAS & SEQPLOT routines as implemented within the EXPGUI-GSAS (v.1251) suite.[37-38] Refinements of monoclinic and orthorhombic phases were performed starting from the atomic models of van Koningsveld *et al*. (1987 and 1990).[9,39] Unit-cell parameters of the starting as-synthesized materials were: *a* =19.9079(2) Å, *b* = 20.1332(2) Å, *c* = 13.3929(2) Å, β = 90.544(1)°, and *V* = 5367.77(15) $Å^3$.[18] In order to have a continuous variation of lattice parameters from monoclinic to orthorhombic ZSM-5 polymorphs, the choice of the space group settings has been varied with respect to that usually reported in literature, *i.e.*, $P12_1/n1$ and *Pmnb* (or $P2_12_12_1$ in the case of toluene containing samples) instead of $P2_1/n11$ and *Pnma* for the monoclinic and the orthorhombic structures, respectively.

Batch method. The adsorption quantity on zeolite were determined by using the batch method. The details on the adsorption conditions as well as the analytical method employed to determine the amount of adsorption at equilibrium, have been previously reported.[5,40] The thermodynamic parameters obtained from linear adsorption isotherms measured at different temperatures were employed to determine the enthalpy and entropy change of the adsorption process.[5] Zeolite samples loaded with TOL, DCE, MTBE, and their mixtures, were prepared by repeating batch adsorption steps on the same zeolite sample. 500 mg of zeolite were placed in a 1 L vessel which was filled to have minimum headspace and equilibrated for 3 hours at a temperature of 25.3(5) °C under continuous stirring (400 rpm). The concentration of contaminants in the aqueous solution was analyzed before and after the contact with the zeolite by Gas Chromatography/Mass Spectroscopy (GC/MS). Details of the analytical methods are reported elsewhere.[5] The procedure was repeated until the concentration of contaminants in the solution no longer decreased after contact with the zeolite. The solids were separated from the aqueous solution by filtration. The solution concentration were 200 mg L^{-1} and 2 mM for the adsorption from unary and binary mixtures, respectively.

RESULTS and DISCUSSION

Patterns evolution at high-temperature. The evolution of part of the collected patterns for samples TOL, TOL-DCE-, DCE, TOL-MTBE, DCE-MTBE, and MTBE, has been preliminarily inspected in *T*-ranges where the $m \leftrightarrow o$ phase transition is expected (*i.e.*, close to the transition

temperatures, T_c, for each investigated sample). Within the compared angular range (i.e., 6.07–6.35 degrees of 2θ), an automatic indexing of the peaks reveals that the 133+13-3 and 313+31-3 doublets of peaks of each zeolite compound gradually move to a single one (i.e., 133 and 313, respectively). Specifically, the gradual overlapping of those doublets highlights on the potential second-order nature (i.e., the first derivative with respect to the temperature T is a continuous function) of the phase transition which characterized all the investigated compounds (by way of example, a cascade plot of the T-dependence for sample TOL, DCE, and MTBE is reported in Figure 1). The estimated transition temperatures, T_c, span within a broad temperature range. Specifically, the estimated T_c is 328±5 K for sample TOL, 333 ±5K for sample TOL-DCE, 348 ±5K for both samples DCE and TOL-MTBE, 353 ± 5K for sample DCE-MTBE, up to 358 ± 5K for sample MTBE.

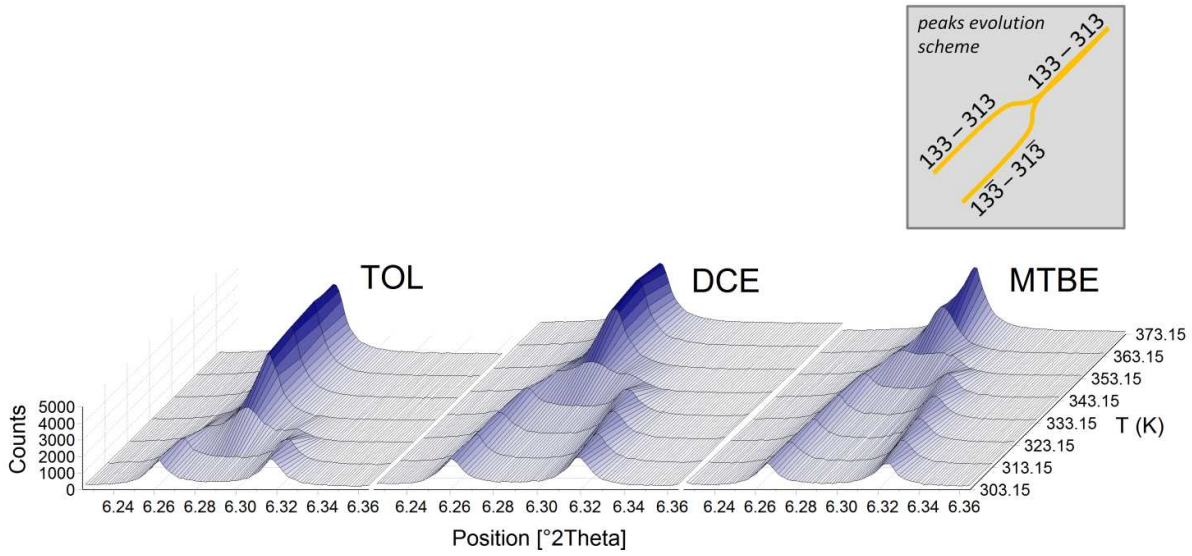

Figure 1. Cascade plot of TOL, DCE, and MTBE doped ZSM-5 samples in the 6.23–6.36 °2θ ranges within the 303–373 K temperature range.

Lattice parameter evolution. The complete set of lattice parameters is given in Table 1 and illustrated as a function of temperature in Figure 2.

Table 1. High-temperature lattice parameters, components of the spontaneous strain tensor ($e_i \times 10^{-3}$), scalar spontaneous strain ($\varepsilon_{ss} \times 10^{-3}$), and volume strain ($V_s \times 10^{-3}$) for all doped ZSM-5 samples. Figures in parentheses represent one standard-deviation error. Detail of the equations employed to calculate the spontaneous strain components are provided as note.

	T(K)	a(Å)	b(Å)	c(Å)	β(°)	V(Å^3)	e_{11} (1)	e_{22} (2)	e_{33} (3)	e_{13} (4)	ε_{ss} (5)	V_s (6)
TOL												
	295	19.9029(3)	20.1173(3)	13.3894(2)	90.578(1)	5360.74(14)	-0.62	0.79	-0.69	-5.04	10.15	-0.61
	303	19.9048(3)	20.1174(3)	13.3915(2)	90.547(2)	5362.15(14)	-0.74	0.93	-0.60	-4.77	9.64	-0.48
	313	19.9098(3)	20.1180(3)	13.3952(2)	90.495(1)	5365.19(15)	-0.71	1.09	-0.40	-4.32	8.74	-0.07
	323	19.9257(4)	20.1017(4)	13.4020(3)	90.111(2)	5368.03(20)	-0.11	0.38	0.07	-0.97	1.98	0.32
	348	19.9344(3)	20.0914(3)	13.4028(2)	90	5367.96(13)	-0.01	-0.01	0.00	0.00	0.01	-0.01
	373	19.9381(3)	20.0923(3)	13.4038(2)	90	5369.59(13)	0.02	0.02	0.00	0.00	0.03	0.04
	398	19.9382(2)	20.0934(2)	13.4044(2)	90	5370.15(11)	-0.02	-0.03	0.01	0.00	0.03	-0.03
	423	19.9375(2)	20.0969(2)	13.4042(2)	90	5370.82(10)	0.00	0.00	0.00	0.00	0.00	-0.01
	448	19.9358(2)	20.0997(2)	13.4036(1)	90	5370.87(08)	0.00	0.00	-0.01	0.00	0.01	-0.01
	473	19.9343(1)	20.1021(1)	13.4028(1)	90	5370.79(07)	0.02	0.03	0.00	0.00	0.03	0.05
	498	19.9328(1)	20.1009(1)	13.4015(1)	90	5369.54(07)	-0.01	-0.01	0.00	0.00	0.02	-0.02

TOL-DCE												
	295	19.9050(3)	20.1175(3)	13.3915(2)	90.590(1)	5362.20(19)	-0.52	-0.15	-1.23	-5.14	10.37	-1.92
	303	19.9073(3)	20.1197(3)	13.3935(2)	90.564(1)	5364.23(19)	-0.61	0.07	-1.12	-4.92	9.92	-1.67
	313	19.9109(3)	20.1210(3)	13.3964(2)	90.525(1)	5366.73(18)	-0.65	0.27	-0.95	-4.58	9.23	-1.33
	323	19.9154(3)	20.1210(3)	13.4002(2)	90.463(1)	5369.51(19)	-0.61	0.38	-0.69	-4.04	8.14	-0.92
	333	19.9290(4)	20.1076(4)	13.4065(3)	90.118(2)	5372.31(26)	-0.08	-0.18	-0.22	-1.03	2.08	-0.48
	348	19.9343(3)	20.1089(3)	13.4095(2)	90	5375.29(18)	0.00	0.00	0.00	0.00	0.01	-0.01
	373	19.9383(3)	20.1064(3)	13.4094(2)	90	5375.66(15)	0.01	0.01	0.01	0.00	0.01	0.03
	398	19.9394(2)	20.1048(2)	13.4084(2)	90	5375.13(14)	0.00	0.00	0.00	0.00	0.01	-0.01
	423	19.9389(2)	20.1040(2)	13.4072(2)	90	5374.30(12)	-0.01	-0.01	0.00	0.00	0.01	-0.02
	448	19.9379(2)	20.1037(2)	13.4058(1)	90	5373.39(10)	0.00	-0.01	0.00	0.00	0.01	-0.01
	473	19.9364(2)	20.1039(2)	13.4045(1)	90	5372.52(09)	0.01	0.02	0.01	0.00	0.02	0.04
	498	19.9349(1)	20.1026(1)	13.4030(1)	90	5371.16(08)	-0.01	-0.01	0.00	0.00	0.01	-0.02
DCE												
	295	19.9028(3)	20.1183(3)	13.3881(2)	90.602(1)	5360.44(19)	-0.11	-1.11	-1.24	-5.25	10.63	-2.47
	303	19.9051(3)	20.1200(3)	13.3903(2)	90.581(1)	5362.42(19)	-0.27	-0.70	-1.13	-5.06	10.22	-2.12
	313	19.9080(3)	20.1219(3)	13.3932(2)	90.550(1)	5364.88(18)	-0.42	-0.26	-0.97	-4.80	9.65	-1.67
	323	19.9116(3)	20.1233(3)	13.3960(2)	90.509(1)	5367.40(18)	-0.50	0.11	-0.79	-4.44	8.93	-1.20
	333	19.9163(3)	20.1240(3)	13.4001(2)	90.443(1)	5370.56(19)	-0.48	0.40	-0.51	-3.86	7.77	-0.60
	343	19.9272(4)	20.1153(4)	13.4065(3)	90.165(2)	5373.83(26)	-0.11	0.17	-0.03	-1.44	2.89	0.02
	348	19.9308(3)	20.1102(3)	13.4068(3)	90	5373.62(20)	0.00	0.01	0.00	0.00	0.01	-0.01
	373	19.9360(3)	20.1046(3)	13.4070(2)	90	5373.60(15)	0.00	0.05	0.01	0.00	0.05	0.04
	398	19.9379(2)	20.1016(2)	13.4061(2)	90	5372.94(14)	0.00	0.03	0.00	0.00	0.03	0.00
	423	19.9377(2)	20.1006(2)	13.4049(2)	90	5372.13(12)	0.00	-0.01	-0.02	0.00	0.02	-0.05
	448	19.9362(2)	20.1023(2)	13.4039(1)	90	5371.80(10)	0.00	0.02	0.00	0.00	0.02	-0.01
	473	19.9343(1)	20.1049(1)	13.4033(1)	90	5371.72(09)	0.00	0.10	0.03	0.00	0.10	0.08
	498	19.9333(1)	20.1034(1)	13.4021(1)	90	5370.58(08)	0.00	0.02	-0.01	0.00	0.02	-0.04
TOL-MTBE												
	295	19.8985(2)	20.1181(2)	13.3847(2)	90.591(1)	5357.88(14)	-0.03	-0.04	-0.66	-5.15	10.33	-0.69
	313	19.9057(3)	20.1205(3)	13.3909(2)	90.528(1)	5362.97(17)	-0.27	0.34	-0.47	-4.61	9.23	-0.38
	323	19.9076(2)	20.1215(2)	13.3925(2)	90.481(1)	5364.47(15)	-0.44	0.51	-0.46	-4.20	8.43	-0.38
	333	19.9145(3)	20.1217(3)	13.3978(2)	90.411(1)	5368.56(17)	-0.33	0.62	-0.16	-3.59	7.21	0.13
	343	19.9199(3)	20.1181(3)	13.4010(2)	90.274(1)	5370.42(19)	-0.24	0.51	0.01	-2.39	4.82	0.28
	348	19.9265(3)	20.1073(3)	13.4013(2)	90	5369.47(16)	0.00	0.01	0.01	0.00	0.01	0.01
	373	19.9316(2)	20.1045(2)	13.4023(2)	90	5370.50(12)	-0.03	-0.03	-0.04	0.00	0.05	-0.10
	398	19.9349(6)	20.1047(6)	13.4036(4)	90	5371.96(39)	0.01	0.02	0.02	0.00	0.03	0.04
	423	19.9343(2)	20.1037(2)	13.4025(1)	90	5371.09(10)	-0.03	-0.04	-0.04	0.00	0.06	-0.12
	448	19.9337(1)	20.1046(1)	13.4023(1)	90	5371.09(09)	-0.01	-0.01	-0.01	0.00	0.01	-0.04
	473	19.9329(1)	20.1051(1)	13.4019(1)	90	5370.85(08)	0.02	0.02	0.02	0.00	0.03	0.03
	498	19.9320(1)	20.1036(1)	13.4010(1)	90	5369.85(08)	0.00	-0.01	-0.01	0.00	0.01	-0.05
DCE-MTBE												
	295	19.9030(3)	20.1191(3)	13.3889(2)	90.603(1)	5361.00(17)	0.50	-1.09	-0.67	-5.26	10.61	-1.27
	313	19.9082(3)	20.1228(3)	13.3938(2)	90.541(1)	5365.45(18)	-0.01	-0.45	-0.69	-4.72	9.47	-1.15
	323	19.9118(3)	20.1237(3)	13.3971(2)	90.502(1)	5368.00(17)	-0.16	-0.20	-0.60	-4.38	8.78	-0.97
	333	19.9149(3)	20.1252(3)	13.3992(2)	90.446(1)	5370.10(17)	-0.29	0.06	-0.56	-3.89	7.81	-0.80
	343	19.9211(3)	20.1256(3)	13.4045(2)	90.369(1)	5374.07(19)	-0.21	0.23	-0.24	-3.22	6.45	-0.23
	348	19.9257(3)	20.1209(3)	13.4071(2)	90.222(1)	5375.18(20)	-0.08	0.07	-0.07	-1.94	3.88	-0.09
	353	19.9269(3)	20.1245(3)	13.4081(2)	90.243(1)	5376.86(19)	-0.10	0.31	-0.02	-2.12	4.25	0.17
	373	19.9348(2)	20.1144(3)	13.4093(2)	90	5376.84(15)	0.05	0.01	0.04	0.00	0.06	0.09
	398	19.9364(2)	20.1109(2)	13.4077(2)	90	5375.68(13)	0.01	-0.01	-0.02	0.00	0.03	-0.03
	423	19.9360(2)	20.1092(2)	13.4059(1)	90	5374.36(11)	0.01	0.00	-0.03	0.00	0.03	-0.03
	448	19.9348(2)	20.1080(2)	13.4043(1)	90	5373.09(10)	0.04	0.00	0.01	0.00	0.04	0.04
	473	19.9339(1)	20.1067(1)	13.4030(1)	90	5371.99(09)	0.07	0.01	0.03	0.00	0.08	0.11
	498	19.9330(1)	20.1042(1)	13.4018(1)	90	5370.60(08)	0.03	0.00	-0.02	0.00	0.04	0.01
MTBE												
	295	19.8993(3)	20.1215(3)	13.3845(2)	90.598(1)	5358.90(17)	0.11	-1.72	-0.68	-5.22	10.59	-2.31
	303	19.9014(3)	20.1229(3)	13.3863(2)	90.580(1)	5360.60(17)	-0.07	-1.24	-0.68	-5.06	10.22	-2.00
	313	19.9045(3)	20.1244(3)	13.3890(0)	90.549(1)	5362.93(17)	-0.23	-0.72	-0.62	-4.79	9.63	-1.58
	323	19.9073(3)	20.1254(3)	13.3916(2)	90.509(1)	5365.02(17)	-0.36	-0.29	-0.55	-4.44	8.91	-1.21
	333	19.9106(3)	20.1259(3)	13.3943(2)	90.462(1)	5367.18(16)	-0.43	0.05	-0.45	-4.03	8.08	-0.84
	343	19.9147(3)	20.1254(3)	13.3979(2)	90.386(1)	5369.63(17)	-0.43	0.29	-0.26	-3.37	6.76	-0.41
	353	19.9235(3)	20.1208(3)	13.4026(2)	90.190(1)	5372.77(19)	-0.15	0.28	0.03	-1.66	3.33	0.15

373	19.9316(2)	20.1094(2)	13.4037(2)	90	5372.37(14)	0.00	0.01	0.02	0.00	0.02	0.01
398	19.9349(2)	20.1069(2)	13.4042(2)	90	5372.79(12)	0.00	0.06	0.00	0.00	0.06	0.02
423	19.9361(2)	20.1055(2)	13.4040(1)	90	5372.66(11)	0.00	0.01	-0.02	0.00	0.02	-0.05
448	19.9360(2)	20.1068(2)	13.4039(1)	90	5372.94(10)	0.01	0.02	0.00	0.00	0.02	-0.01
473	19.9347(1)	20.1090(1)	13.4036(1)	90	5373.06(09)	0.00	0.07	0.02	0.00	0.08	0.05
498	19.9338(1)	20.1076(1)	13.4028(1)	90	5372.12(08)	0.00	0.03	-0.01	0.00	0.03	-0.02

Notes: the listed components of the spontaneous strain tensor have been calculated as:

$$e_{11} = a/a_0 - 1 \quad (1)$$

$$e_{22} = b/b_0 - 1 \quad (2)$$

$$e_{33} = (c/c_0 \sin\beta) - 1 \quad (3)$$

$$e_{13} = \tfrac{1}{2} (c/c_0 \cos\beta) \quad (4)$$

$$\varepsilon_{ss} = (e_{11}^2 + e_{22}^2 + e_{33}^2 + 2e_{13}^2)^{1/2} \quad (5)$$

$$V_s = V/V_0 - 1 \quad (6)$$

where a_0, b_0, c_0, and V_0 are the extrapolated unit-cell parameters of the paraelastic phase into the stability field of the ferroelastic phase; the spontaneous strain tensors e_{12} and e_{23} are equal to zero.[41]

The lattice parameters variation with temperature of the investigated samples outlines trends with similar features which reflect those previously reported for the unloaded ZSM-5.[18] An inspection of Figure 2 reveals that each sample is characterized by lattice parameters that vary continuously on increasing temperature, but a strong change in their evolution can be recognized close to the temperature at which the monoclinic to orthorhombic phase transition takes place (*i.e.*, $T \approx T_c$). Specifically, within the stability field of the monoclinic phase (*i.e.*, for $T < T_c$), the ZSM-5 host structure has an anisotropic answer to the temperature increasing. The lattice parameters undergo a very rapid change, with *a* and *c* cell-axes that expand by the same rate, whereas the *b*-axis undergoes an equivalent but opposite variation. At higher temperatures (*i.e.*, for $T > T_c$), within the stability field of the orthorhombic phase, the lattice parameters vary more gradually. Indeed, up to the maximum temperature is reached, the unit-cell axes show almost constant values which define subparallel trends.

Besides those considerations, as expected from the symmetries involved in the ferroelastic to the paraelastic ZSM-5 phase transition,[18] the main lattice changes are related to the variation of the monoclinic angle, β. On average, each sample shows a variation of the monoclinic angle 4 times higher to that of the unit-cell axes.

The sum of the above described lattice variations is schematized by the evolution of the unit-cell volume, *V* (see Table 1). Indeed, at temperatures lower than that of transition, each sample records a strong volume expansion (on average ≈ 0.25 % with respect to the volume at *RT*). At higher temperatures (*i.e.*, $T > T_c$), the volume values fluctuate around the maximum value reached or undergo a mild decrease (in this *T* range, the mean volumetric variation is ≈ 0.06 %).

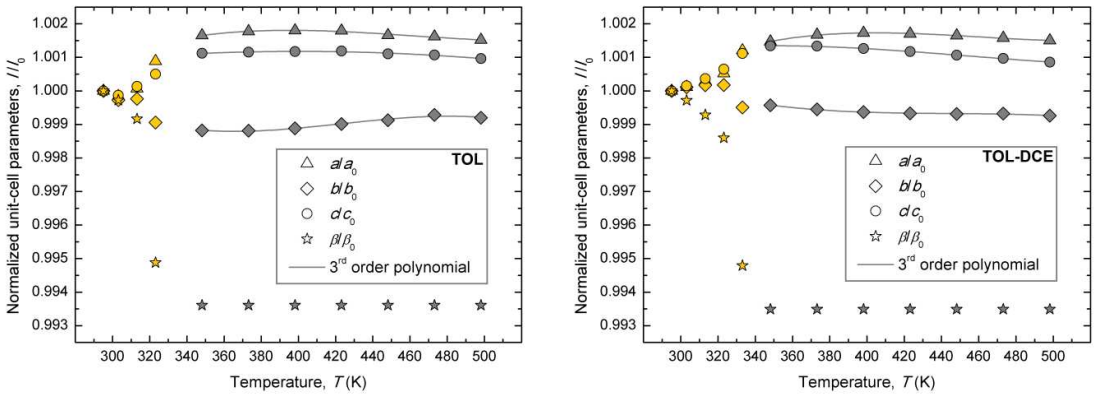

A B

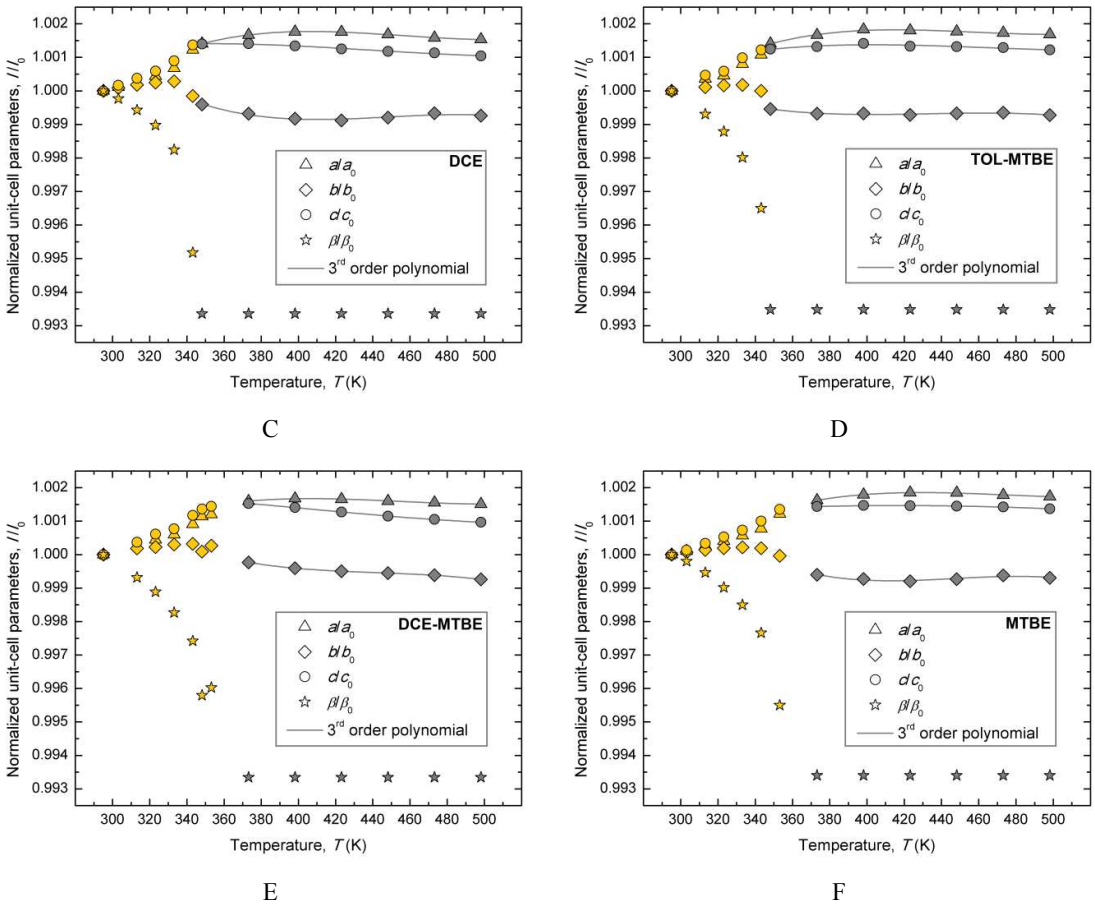

Figure 2 (A-F). Temperature dependence of lattice parameters (normalized unit-cell axes and β angle) obtained during heating cycles from room temperature to 498 K for the ZSM-5 zeolites with TOL (A), TOL-DCE (B), DCE (C), TOL-MTBE (D), DCE-MTBE (E), and MTBE (F), as adsorbed molecules. Yellow filled symbols refer to lattice parameters of the monoclinic structure, whereas gray filled symbols are those of the orthorhombic structure after the phase transition. Standard-deviation errors are within the symbol size. Solid lines through gray symbols are those fitted to a third-order polynomial equation.

Thermal analyses. As reported in previous works,[2,4,5,42] within the stability field of the monoclinic phase (*i.e.*, for $T < T_c$), no changes in the extraframework site occupancies are observed. Specifically, under the assumption of guest organic molecules exclusively localized within the host ZSM-5 zeolite framework, it has been observed that up to the transition temperature the number of guest molecules per unit-cell is almost unchanged with respect to that found at room temperature. This evidence suggests that the transient framework expansion cannot be related to the desorption of extraframework species (organics and/or water molecules). In Figure 3, the variation of the mass weight loss (TG) and its derivative (DTG) for TOL, DCE, and MTBE unary (Figure 3A) and TOL-DCE, TOL-MTBE, and DCE-MTBE binary (Figure 3B) mixtures is plotted as a function of temperature up to 500 K.

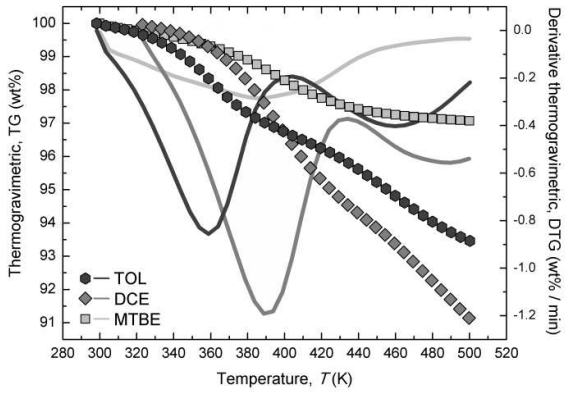

A

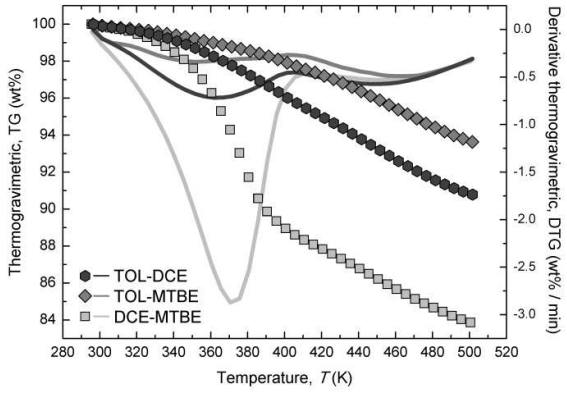

B

Figure 3 (A-B). Simultaneous thermogravimetric (TG; symbols) and derivative thermogravimetric (DTG; continuous lines) analyses of the investigated ZSM-5 samples with unary (A) and binary (B) adsorbed molecules in the temperature range 295−500 K.

According to those investigations,[2,4,5,42] the first DTG peak can be ascribed to the desorption of species bounded to the sample surface (water molecules and/or embedded organic species). On the contrary, the desorption of guest molecules embedded in the ZSM-5 channels occurs at higher temperature and their mobility inside the framework is controlled by configurational effects.[5] As a matter of fact, refined bond distances indicate that the extraframework species interact with co-adsorbed water molecules thus forming organic–water oligomers (clusters or short chains) interacting with the framework oxygens.[1-4,31] According to the literature,[4,5,43-48] this result suggests that the monoclinic ferroelastic phase shows an initial breathing to a "pore-mouth-breathing motion" due to the weakening of hydrogen bonding network (host-guest interactions). After the ferroelastic to the paraelastic phase transition, a sudden slope change in the unit-cell parameters occurs and the release/decomposition of guest organic molecules takes place. As depicted in Figure 3B, this finding is also confirmed for the examined TOL-DCE, TOL-MTBE, and DCE-MTBE binary mixtures. Whether a slight difference in the TG curves can be highlighted with respect to those of previous investigations (*e.g.*, references 2,4, and 5), this difference can be readily explained considering that the analyzed samples have been loaded with organic molecules by means of the previously described batch method twice, *i.e.*, before the thermogravimetric analyses and the XRPD synchrotron experiments, respectively. The fluctuation of the maximum slope change in the lattice parameters at the $m \leftrightarrow o$ phase transition of the loaded ZSM-5 zeolite structure can be related to the different framework-extraframework binding energy (MTBE > DCE > TOL). Into the temperature

regime of the paraelastic phase, the host-host and host-guest interactions are released, and a new transient deformation opening and distortion of the pore apertures occurs.

Strain analysis and character of the phase transition. As reported in the introductive section, it has been recently demonstrated that the lattice parameters variation at the *m*↔*o* phase transition (*i.e.*, from the ferroelastic to the paraelastic phase) of an undoped ZSM-5 zeolite structure can be interpreted through the Landau theory using the concept of spontaneous strain.[18] Formally, the spontaneous strain is an excess property, a second-rank tensor for which (depending to the constraints of symmetry) up to six independent strain components have to be determined in order to quantify the excess free energy associated with the phase transition.[41] The components of the spontaneous strain tensor have to be calculated by extrapolating the lattice parameters of the paraelastic phase into the temperature regime of the ferroelastic phase.[49]

As depicted in Figure 2, all the investigated ZSM-5 samples undergo a *m*↔*o* phase transition at temperatures that are far from a possible saturation of the thermal expansion.[50] Therefore, the temperature evolution of the paraelastic phase can be properly described using a third-order polynomial expression (the resulting fits of the polynomial regression to the lattice parameters at $T > T_c$ are visualized as solid curves in Figure 2). The calculated strains e_i, ε_{ss}, and V_s, are listed in Table 1 and visualized as a function of temperature in Figure 4 (A, C, E, G, I, and K).

Described as tricritical,[18] and reversible with displacive features,[18,20] the *m*↔*o* phase transition sets the ZSM-5 structure as a ferroelastic material which belongs to the "Aizu-type" *mmm***F**2/*m*,[51] meaning that, when the point group *mmm* (orthorhombic) changes into 2/*m* (monoclinic), the primary order parameter, Q, behaves as the symmetry-adapted strain.[41,49] For the *m*↔*o* phase transitions of all the samples here investigated, the ferroelastic operator **F** describes a proper spontaneous strain where the order parameter have to be coupled with the largest component of the spontaneous strain,[49,51] *i.e.*, the shear strain e_{13} derived from the variation of the monoclinic β angle (see Table 1).

It is now possible employ a model based on the Landau theory to describe the excess thermodynamic quantities. Through a 246 Landau potential of the order parameter Q, with form:[18,41,49,52]

$$G(Q) = A/2(T-T_c)Q^2 + B/4Q^4 + C/6Q^6 \qquad (7)$$

fits shown by solid lines in Figure 4 (B, D, F, H, J, and L) are obtained for the reported transition temperatures, T_c, and Landau coefficients ratios, B/A and C/A.

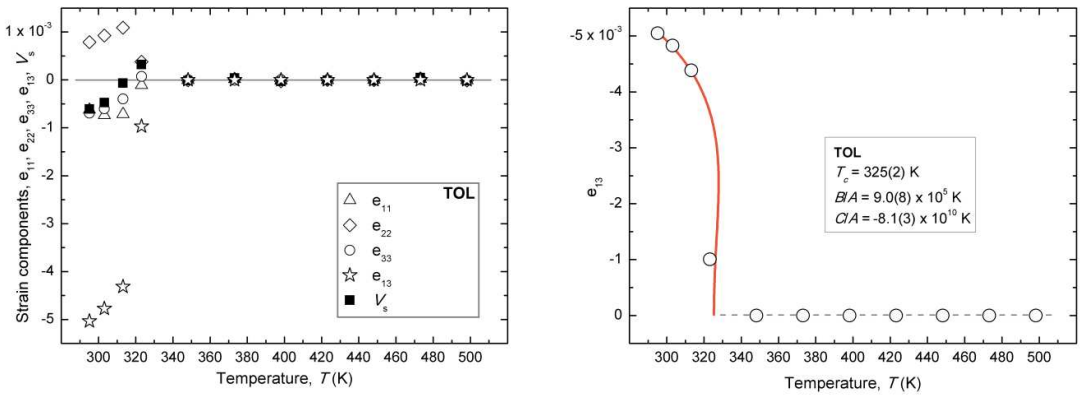

A B

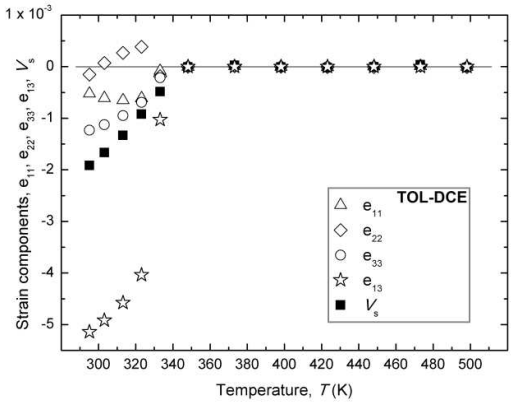
1 x 10⁻³
Strain components, e11, e22, e33, e13, Vs
Temperature, T (K)
TOL-DCE
e11
e22
e33
e13
Vs

C

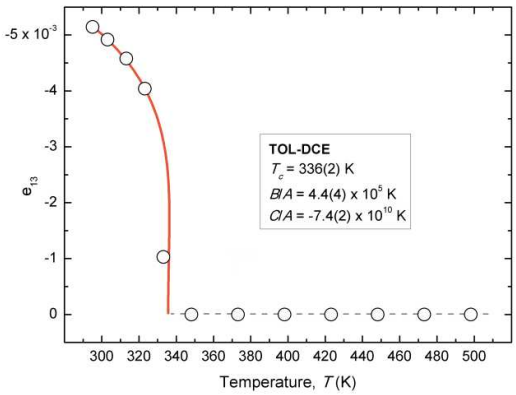
-5 x 10⁻³
e13
Temperature, T (K)
TOL-DCE
Tc = 336(2) K
B/A = 4.4(4) x 10⁵ K
C/A = -7.4(2) x 10¹⁰ K

D

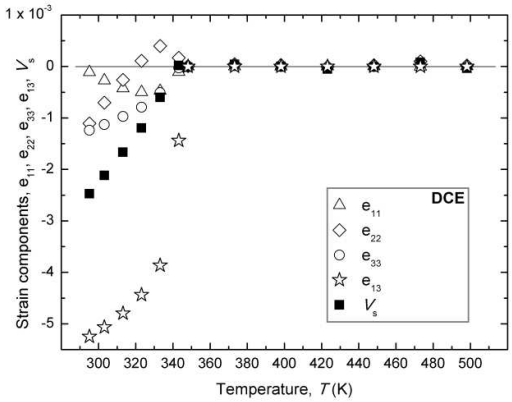
1 x 10⁻³
Strain components, e11, e22, e33, e13, Vs
Temperature, T (K)
DCE
e11
e22
e33
e13
Vs

E

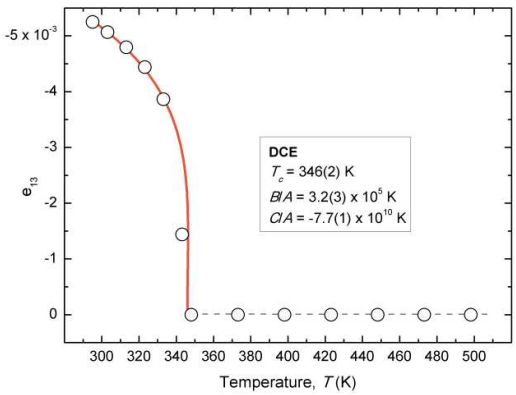
-5 x 10⁻³
e13
Temperature, T (K)
DCE
Tc = 346(2) K
B/A = 3.2(3) x 10⁵ K
C/A = -7.7(1) x 10¹⁰ K

F

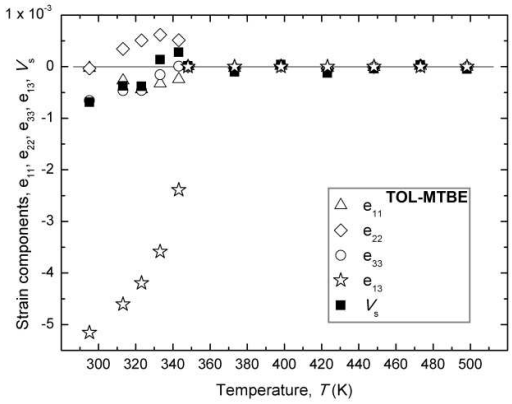
1 x 10⁻³
Strain components, e11, e22, e33, e13, Vs
Temperature, T (K)
TOL-MTBE
e11
e22
e33
e13
Vs

G

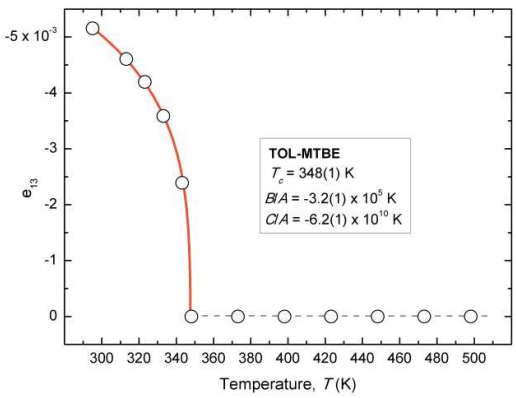
-5 x 10⁻³
e13
Temperature, T (K)
TOL-MTBE
Tc = 348(1) K
B/A = -3.2(1) x 10⁵ K
C/A = -6.2(1) x 10¹⁰ K

H

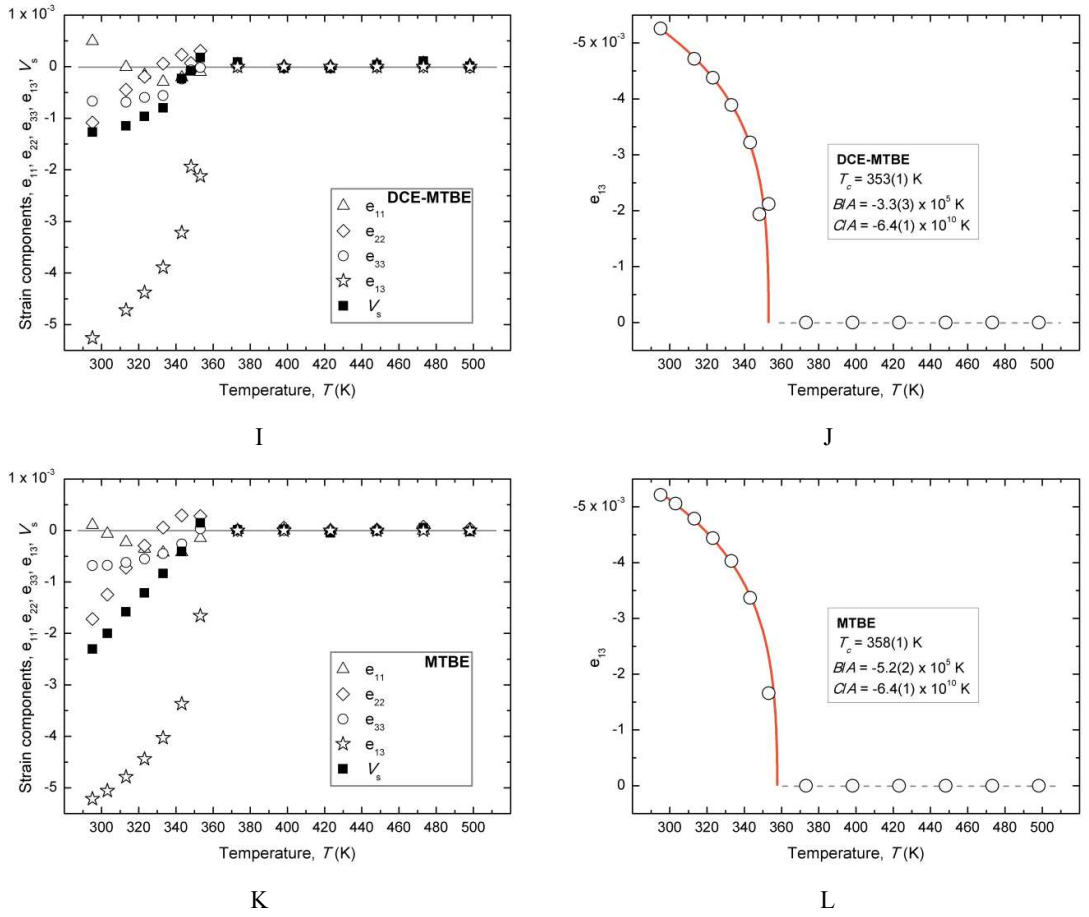

Figure 4 (A-L). Temperature dependence of spontaneous strain components and volume strain due to the *m*↔*o* phase transition in doped ZSM-5 structures (A, C, E, G, I, and K; cfr. Equations 1–4, and 6) coupled with the temperature dependence of the largest spontaneous strain tensor component e_{13}, which behaves as the primary order parameter Q for each phase transition (B, D, F, H, J, and L; cfr. Equation 7).

Despite the wide temperature range at which the phase transitions are observed (*i.e.*, from 325 K to 358 K for the TOL and MTBE samples, respectively), the calculated ratios of the Landau coefficients for all the doped ZSM-5 samples have the same order of magnitude with $C/A >> B/A$ in absolute value, and provide common information on the ferroelastic-paraelastic phase transition. In particular, the shear strain component e_{13} of any ZSM-5 sample has a continuous dependence on temperature (*i.e.*, the Q evolution in Figure 4 presents no jumps), meaning that the first derivative of the free energy $\partial G/\partial T$ is continuous, and first-order phase transitions do not take place.

As it was reported for the undoped ZSM-5, those features suggest that the *m*↔*o* phase transition of any ZSM-5 doped sample is tricritical.[18] If true, the temperature dependence of Q up to $T = T_c$ should follow the relationship:

$$Q = |(T_c - T)/T_c|^n \qquad (8)$$

with $n \rightarrow ¼$.[52]

In Figure 5, the variation of the normalized order parameter, $(Q / Q_0)^4$, and that of the normalized monoclinic angles, (β / β_0), where Q_0 and β_0 are both extrapolated at 0 K, for the six doped ZSM-5 samples are plotted as a function of the normalized transformation temperature (T / T_c, for $T < T_c$). Both images in Figure 5 unequivocally show that, upon heating, all the data under comparison lie over those curves defined by a transition which can be ascribed as tricritical.[49,53]

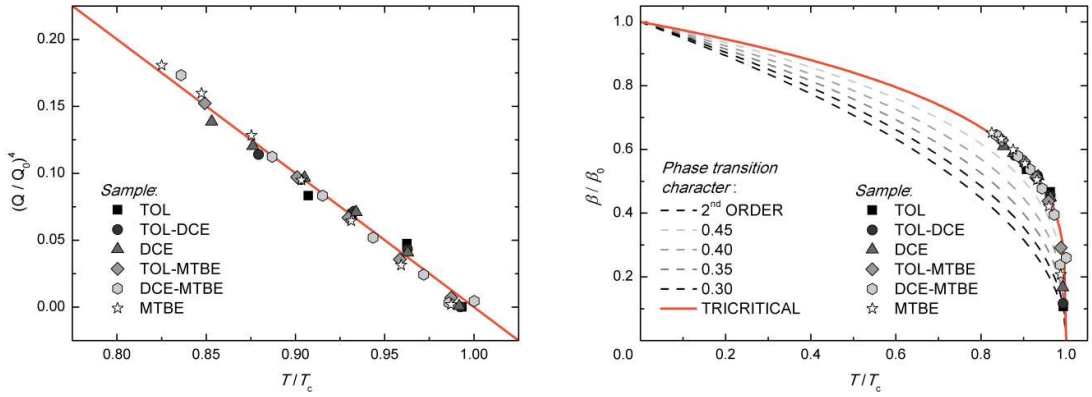

A B

Figure 5 (A-B). (A) Normalized order parameter, $(Q / Q_0)^4$, and (B) normalized monoclinic angles, (β / β_0), as a function of the normalized transformation temperature (T / T_c, for $T < T_c$).

Thermodynamic of the adsorption process. In the following section only the ZSM-5 loaded with unary mixtures were considered.

The transition temperature (T_c) of ZSM-5 samples saturated with the three pure organic contaminants (TOL, DCE, and MTBE) along with their boiling point (T_b) and their vaporization enthalpy (ΔH_{vap}) are reported in Table 2.

Table 2. Transition temperature (T_c), calculated ratio of the *C*/*A* Landau coefficients, boiling point of organic compounds (T_b), enthalpy of molecular vaporization (ΔH_{vap}), experimental enthalpy of molecular adsorption (ΔH_{ad} from aqueous solution), calculated entropy of molecular adsorption (ΔS_{ad} from aqueous solution), and experimental Gibbs free energy of adsorption (ΔG_{ad} from aqueous solution) for ZSM-5 samples saturated with unary mixture of contaminants (for details see ref. 5). Figures in parentheses represent one standard-deviation error.

	T_c (K)	C/A ($\times 10^{10}$K)	T_b (K)	ΔH_{vap} (kJ mol^{-1})	$\Delta H_{ad}(exp)$ (kJ mol^{-1})	$\Delta S_{ad}(calc)$ (J mol^{-1} K^{-1})	$\Delta G_{ad}(exp)$ (kJ mol^{-1})
TOL	325(2)	-8.1(3)	384	-37	-42	82	-66
TOL-DCE	336(2)	-7.4(2)					
DCE	346(2)	-7.7(1)	357	-35	-33	57	-50
TOL-MTBE	348(1)	-6.2(1)					
DCE-MTBE	353(1)	-6.4(1)					
MTBE	358(1)	-6.4(1)	328	-30	-28	72	-49

Data in Table 2 reveal that the *m*↔*o* phase transition of TOL and DCE takes place at temperatures below the boiling point of the guest molecules. This finding well agree with thermogravimetric data reported in Figure 3A, where no desorption of guest molecules embedded in the channels is observed for $T < T_c$.

In order to evaluate a possible correlation between the temperature at which the ZSM-5 *m*↔*o* phase transition occurs and the guest molecules adsorption process, the entropy (ΔS_{ad}) and the enthalpy (ΔH_{ad}) of adsorption along with the boiling point (T_b) for TOL, DCE, and MTBE are plotted in Figure 6 as a function of T_c. By inspecting Figure 6 emerges that ΔH_{ad} directly scales with T_c, and consequently with ΔH_{vap}. Specifically, the higher T_c corresponds to the ZSM-5 loaded with the

organic contaminant with the lower boiling point (*e.g.*, MTBE). On the contrary, the lowest T_c corresponds to the highest entropy of adsorption (ΔS_{ad}).

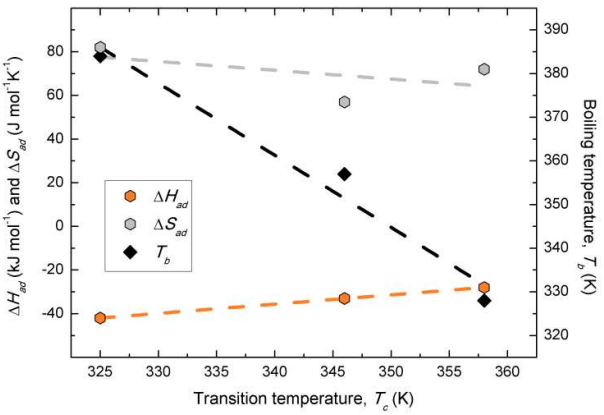

Figure 6. Boiling point temperature (T_b), enthalpy (ΔH_{ad}) and entropy (ΔS_{ad}) of the adsorption of TOL, DCE, and MTBE from aqueous solution as a function of the transition temperature (T_c).

A parallel comparison between thermogravimetric analysis and results from the adsorption processes suggests that the *m*↔*o* phase transition of the investigated ZSM-5 samples is not directly induced by the release of the adsorbed molecules. Indeed, it seems that by increasing the binding energy of the guest molecule the transition enthalpy of ZSM-5 decreases. On the basis of this correlation, stronger host-host or host-guest interactions appear to favor lattice strains which induce the *m*↔*o* phase transition.

CONCLUDING REMARKS

In this contribution has been highlighted how the adsorption of different organic contaminants can strongly affect the temperature of transition and the thermodynamic features related with the monoclinic to orthorhombic phase transition of highly siliceous ZSM-5 zeolites.

In particular, although the tricritical character of the *m*→*o* phase transition is constant for all the investigated compounds, the occurrence of strong interactions among host structure (*i.e.*, the ZSM-5 zeolite) and guest molecules (*i.e.*, organic contaminants as toluene, 1,2-dichloroethane, methyl-tert-buthyl-ether, and a binary mixtures of them) has been emphasized through thermodynamic evidences such as the lattice distortion described with the spontaneous strain correlated to the zeolite phase transition, and the enthalpy and entropy of organic molecules adsorption.

Once the nature of the phase transition is known, and assuming it as purely tricritical (i.e. the *B* coefficient in Equation 7 is negligible), the excess free energy expression derived by the Landau potential can be simplified as:

$$G(Q) = A/2(T-T_c)Q^2 + C/6Q^6 \qquad (10)$$

Consequently, the equilibrium variation of the primary order parameter Q with T is:[52]

$$Q = A/C(T-T_c)^{1/4} \qquad \text{with } T_c = C/A \qquad (11)$$

The equivalence between transition temperature T_c and ratio of the C/A Landau coefficients in the Equation 11 is well described by data listed in Table 2 and plotted in Figure 7A.

Furthermore, it is known that the Landau coefficients incorporate all the several factors that contribute to the free energy change during a phase transition.[41,49,52] With reference to the investigated ZSM-5 samples, the contribution of the lattice change due to the $m \rightarrow o$ phase transition is included in the Landau coefficients A and C, the latter incorporating the excess enthalpy part (ΔH_{exc}) of the free energy expansion.
Figure 7B clearly shows that the excess enthalpy part (ΔH_{exc}) of the free energy expansion is strictly related with the enthalpy of guest molecules adsorption.

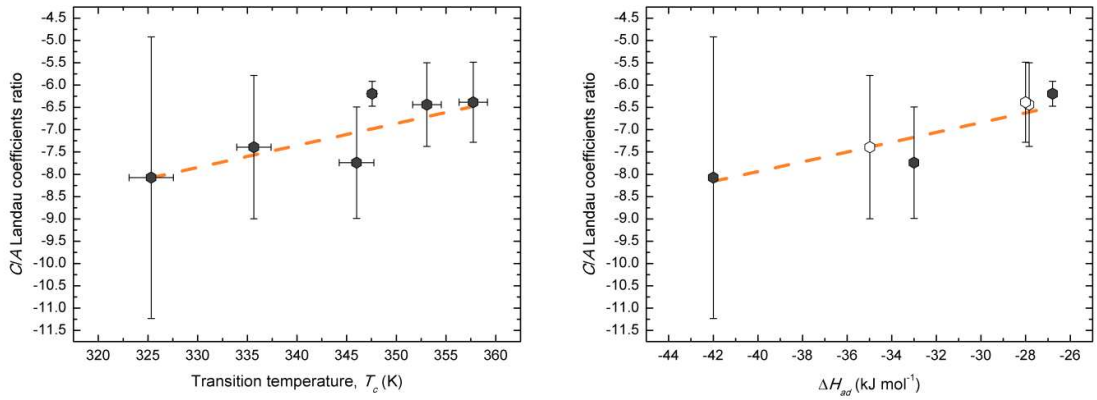

Figure 7 (A-B). (A) Monoclinic-orthorhombic $m \leftrightarrow o$ phase transition temperature (T_c), and (B) enthalpy (ΔH_{ad}) of the adsorption of organic contaminants for the ZSM-5 investigated vs calculated ratio of the C/A Landau coefficients (cfr. Equation 7). Empty symbols in B refer to ΔH_{ad} data extrapolated from equation 11.

ACKNOWLEDGEMENTS
This study was carried out within the "ZAPPING" project (high-pressure nano-confinement in Zeolites: the mineral science know-how APPlied to engineerING of innovative materials for technological and environmental applications) founded by the PRIN2015 program of the Italian Ministry for University and Research (MIUR).

REFERENCES
(1) Martucci, A.; Braschi, I.; Bisio, C.; Sarti, E.; Rodeghero, E.; Bagatin, R.; Pasti, L. Influence of water on the retention of methyl tertiary-butyl ether by high silica ZSM-5 and Y zeolites: a multidisciplinary study on the adsorption from liquid and gas phase. *RSC Adv.* **2015**, *5*, 86997−87006.
(2) Martucci, A.; Rodeghero, E.; Pasti, L.; Bosi, V.; Cruciani, G. Adsorption of 1,2-dichloroethane on ZSM-5 and desorption dynamics by in situ synchrotron powder X-ray diffraction. *Micropor. Mesopor. Mat.* **2015**, *215*, 175−182.
(3) Pasti, L.; Rodeghero, E.; Sarti, E.; Bosi, V.; Cavazzini, A.; Bagatin, R.; Martucci, A. Competitive adsorption of VOCs from binary aqueous mixtures on zeolite ZSM-5. *RSC Adv.* **2016**, *6*, 54544−54552.
(4) Rodeghero, E.; Martucci, A.; Cruciani, G.; Bagatin, R.; Sarti, E.; Bosi, V.; Pasti, L. Kinetics and dynamic behaviour of toluene desorption from ZSM-5 using in situ high-temperature synchrotron powder X-ray diffraction and chromatographic techniques. *Catal. Today* **2016**, *277*, 118−125.
(5) Rodeghero, E.; Martucci, A.; Cruciani, G.; Sarti, E.; Cavazzini, A.; Costa, V.; Bagatin, R.; Pasti, L. Detailed investigation of thermal regeneration of high-silica ZSM-5 Zeolite through in situ

synchrotron X-ray powder diffraction and adsorption studies. J. Phys. Chem. C **2017**, *121*, 17958−17968.
(6) Baerlocher, C.; McCusker, L. B.; Olson, D. H. Atlas of zeolite framework types, 6th ed.; Elsevier: Amsterdam, 2007.
(7) Kokotailo, G. T.; Lawton, S. L.; Olson, D. H.; Meier, W. M. Structure of synthetic zeolite ZSM-5. *Nature* **1978**, *272*, 437−438.
(8) van Koningsveld, H.; Tuinstra, F. The location of p-Xylene in a single crystal of zeolite H-ZSM-5 with a new, sorbate-induced, orthorhombic framework symmetry. *Acta Crystallogr.* **1989**, *B45*, 423−431.
(9) van Koningsveld, H.; Jansen, J. C.; van Bekkum, H. The monoclinic framework structure of zeolite H-ZSM-5. Comparison with the orthorhombic framework of as-synthesized ZSM-5. *Zeolites* **1990**, *10*, 235−242.
(10) van Koningsveld, H.; Jansen, J. C.; van Bekkum, H. The orthorhombic/monoclinic transition in single crystals of zeolite ZSM-5. *Zeolites* **1987**, *7*, 564−568.
(11) van Koningsveld, H.; Tuinstra, F.; Jansen, J. C.; van Bekkum, H. On the preparation of a monoclinic (nearly) single crystal of zeolite H-ZSM-5. *Zeolites* **1989**, *9*, 253−256.
(12) van Koningsveld, H. High-temperature (350 K) orthorhombic framework structure of zeolite H-ZSM-5. *Acta Crystallogr.* **1990**, *B46*, 731−735.
(13) Millini, R.; Previde Massara, E.; Perego, G.; Bellussi, G. Framework composition of titanium silicalite-1. *J. Catal.* **1992**, *137*, 497−503.
(14) Lamberti, C.; Bordiga, S.; Zecchina, A.; Carati, A.; Fitch, A. N.; Artioli, G.; Petrini, G.; Salvalaggio, M.; Marra, G. L. Structural characterization of Ti-silicalite-1: A synchrotron radiation X-Ray powder diffraction study. *J. Catal.* **1999**, *183*, 222−231.
(15) Artioli, G.; Lamberti, C.; Marra, G. L. Neutron powder diffraction study of orthorhombic and monoclinic defective silicalite. *Acta Crystallogr.* **2000**, *B56*, 2−10.
(16) Kamiya, N.; Yano, M.; Matsuo, H.; Iwama, W.; Nishi, K.; Yokomori, Y. Simple method for preparing monoclinic single crystals of zeolite ZSM-5 and analysis of their structure. *Z. Kristallogr.* **2010**, *225*, 139−145.
(17) Leardini, L.; Martucci, A.; Cruciani, G. The unusual thermal behaviour of boron-ZSM-5 probed by "*in situ*" time-resolved synchrotron powder diffraction. *Micropor. Mesopor. Mater.* **2013**, *173*, 6−14.
(18) Ardit, M.; Martucci, A.; Cruciani, G. Monoclinic-orthorhombic phase transition in ZSM-5 zeolite: spontaneous strain variation and thermodynamic properties. *J. Phys. Chem. C* **2015**, *119*, 7351–7359.
(19) Marra, G. L.; Tozzola, G.; Leofanti, G.; Padovan, M.; Petrini, G.; Genoni, F.; Venturelli, B.; Zecchina, A.; Bordiga, S.; Ricchiardi, G. Orthorhombic and monoclinic silicalites: structure, morphology, vibrational properties and crystal defects. *Stud. Surf. Sci. Catal.* **1994**, *84*, 559−566.
(20) Wu, E. L.; Lawton, S. L.; Olson, D. H.; Rohrman, A. C.; Kokotailo, G. T. ZSM-5-type materials. Factors affecting crystal symmetry. *J. Phys. Chem.* **1979**, *83*, 2777−2781.
(21) Hay, D. G.; Jaeger, H.; West, G. W. Examination of the monoclinic/orthorhombic transition in silicalite using XRD and silicon NMR. *J. Phys. Chem.* **1985**, *89*, 1070−1072.
(22) Endoh, A. Calorimetric study of the monoclinic-orthorhombic phase transition in highly siliceous zeolite ZSM-5. *Zeolites* **1988**, *8*, 250−251.
(23) Mentzen, B. F.; Sacerdote-Peronnet, M. Flexibility of the framework structure in highly crystalline silicalite during the reversible monoclinic/orthorhombic solid state polymorphic phase transition. *Mater. Res. Bull.* **1993**, *28*, 1017−1024.
(24) Mentzen, B. F.; Letoffe, J.-M.; Claudy, P. Enthalpy change and temperature of the reversible monoclinic-orthorhombic phase transition in MFI type zeolitic materials. *Thermochim. Acta* **1996**, *288*, 1−7.

(25) van Koningsveld, H.; Jansen, J. C.; de Man, A. J. M. Single-crystal structure analysis and energy minimizations of a MFI-type zeolite at low p-dichlorobenzene sorbate loading. *Acta Crystallogr.* **1996**, *B52*, 131−139.
(26) van Koningsveld, H.; Jansen, J. C.; van Bekkum, H. The location of p-dichlorobenzene in a single crystal of zeolite H-ZSM-5 at high sorbate loading. *Acta Crystallogr.* **1996**, *B52*, 140−144.
(27) van Koningsveld, H.; Koegler, J. H. Preparation and structure of crystals of zeolite H-ZSM-5 loaded with p-nitroaniline. *Micropor. Mater.* **1997**, *9*, 71−81.
(28) Nishi, K.; Hidaka, A.; Yokomori, Y. Structure of toluene6.4-ZSM-5 and the toluene disproportionation reaction on ZSM-5. *Acta Crystallogr.* **2005**, *B61*, 160−163.
(29) Nishi, K.; Yokomori, Y. Determining the structure of a benzene7.2-silicalite-1 zeolite using a single-crystal X-ray method. *Acta Crystallogr*. **2011**, *B67*, 508−515.
(30) Martucci, A.; Pasti, L.; Nassi, M.; Alberti, A.; Arletti, R.; Bagatin, R.; Vignola, R.; Sticca, R. Adsorption mechanism of 1,2-dichloroethane into an organophilic zeolite mordenite: a combined diffractometric and gas chromatographic study. *Micropor. Mesopor. Mater.* **2012**, *151*, 358−367.
(31) Pasti, L.; Martucci, A.; Nassi, M.; Cavazzini, A.; Alberti, A.; Bagatin, R. The role of water in DCE adsorption from aqueous solutions onto hydrophobic zeolites. *Micropor. Mesopor Mater.* **2012**, *160*, 182−193.
(32) Fujiyama, S.; Kamiya, N.; Nishi, K.; Yokomori, Y. Location of CO_2 on silicalite-1 zeolite using a single-crystal X-ray method. *Z. Kristallogr.* **2013**, *228*, 180−186.
(33) Kamiya, N.; Oshiro, T.; Tan, S.; Nishi, K.; Yokomori, Y. Adsorption process of phenol on silicalite-1 and crystal structure of phenol8.0−silicalite-1 using a single crystal X-ray diffraction method. *Micropor. Mesopor. Mater.* **2013**, *169*, 168−175.
(34) Cha, W.; Jeong, N. C.; Song, S.; Park, H.; Thanh Pham, T. C.; Harder, R.; Lim, B.; Xiong, G.; Ahn, D.; McNulty, I.; et al. Core-shell strain structure of zeolite microcrystals. *Nat. Mater.* **2013**, *12*, 729−734.
(35) Boerio-Goates, J.; Stevens, R.; Hom, B. K.; Woodfield, B. F.; Piccione, P. M.; Davis M. E.; Navrotsky, A. Heat capacities, third-law entropies and thermodynamic functions of SiO_2 molecular sieves from $T = 0$ to 400 K. *J. Chem. Thermodyn*. **2002**, *34*, 205−227.
(36) Martucci, A.; Pasti, L.; Marchetti, N.; Cavazzini, A.; Dondi, F.; Alberti, A. Adsorption of pharmaceuticals from aqueous solutions on synthetic zeolites. *Micropor. Mesopor. Mater.* **2012**, *148*, 174−183.
(37) Larson, A. C.; Von Dreele, R. B. *General structure analysis system (GSAS)*; Los Alamos National Laboratory Report LAUR: 86-748, 2004.
(38) Toby, B. H. *EXPGUI*, a graphical user interface for *GSAS*. *J. Appl. Crystrallogr.***2001**, *34*, 210–213.
(39) van Koningsveld, H.; van Bekkum, H.; Jansen, J. C. On the location and disorder of the tetrapropylammonium (TPA) ion in zeolite ZSM-5 with improved framework accuracy. *Acta Cryst.* **1987**, *B43*, 127–132.
(40) Arletti, R.; Martucci, A.; Alberti, A.; Pasti, L.; Nassi, M.; Bagatin, R. Location of MTBE and toluene in the channel system of the zeolite mordenite: Adsorption and host–guest interactions. *J. Solid State Chem.* **2012**, 194, 135–142.
(41) Carpenter, M. A.; Salje, E. K. H.; Graeme-Barber, A. Spontaneous strain as a determinant of thermodynamic properties for phase transitions in minerals. *Eur. J. Mineral.* **1998**, *10*, 621–691.
(42) Rodeghero, E.; Pasti, L.; Sarti, E.; Cruciani, G.; Bagatin, R.; Martucci, A.. Temperature-induced desorption of Methyl tert-Butyl Ether confined on ZSM-5: An in situ synchrotron XRD powder diffraction study. *Minerals* **2017**, 7, 34–42.
(43) Felsche, J.; Luger, S.; Baerlocher, Ch. Crystal structures of the hydro-sodalite $Na_6[AlSiO_4]_6$ $8H_2O$ and of the anhydrous sodalite $Na_6[AlSiO_4]_6$. *Zeolites* **1986**, 6, 367–372.
(44) Cruciani, G.; Gualtieri, A. Dehydration dynamics of analcime by in situ synchrotron powder diffraction. *Am. Mineral.* **1999**, *84*, 112–119.

(45) Seryotkin, Y. V.; Joswig, W.; Bakakin, V. V.; Belitsky, I. A.; Fursenko, B. A. High-temperature crystal structure of wairakite. *Eur. J. Mineral.* **2003**, *15*, 475–484.
(46) Leardini, L.; Martucci, A.; Cruciani, G. The unusual thermal expansion of pure silica sodalite probed by in situ time-resolved synchrotron powder diffraction. *Micropor. Mesopor. Mat.* **2012**, *151*, 163–171.
(47) Martucci, A.; Rodeghero, E.; Cruciani, G. Continuous dehydration of cavansite under dynamic conditions: an in situ synchrotron powder-diffraction study. *Eur. J. Mineral.* **2016**, *28*, 5–13.
(48) Vignola, R.; Cova, U.; Fabiani, F.; Sbardellati, T.; Sisto, R. Process for the regeneration of non-polar adsorbing zeolites used for the treatment of contaminated water. Patent publication number: WO, 2009000429 2009, A1.
(49) Salje, E. K. H. *Phase transition in ferroelastic and co-elastic crystals*; Cambridge University Press: Cambridge, 1990.
(50) Salje, E. K. H.; Wruck, B.; Thomas, H. Order-parameter saturation and low-temperature extension of Landau theory. *Z. Phys. B Con. Mat.* **1991**, *82*, 399–404.
(51) Aizu, K. Determination of the state parameters and formulation of spontaneous strain for ferroelastics. *J. Phys. Soc. Jpn*. **1970**, *28*, 706–716.
(52) Putnis, A. *Introduction to mineral sciences*; Cambridge University Press: Cambridge, 1992.
(53) Shian, S.; Sarin, P.; Gurak, M.; Baram, M.; Kriven, W. M; Clarke, D. R. The tetragonal–monoclinic, ferroelastic transformation in yttrium tantalate and effect of zirconia alloying. *Acta Mater*. **2014**, *69*, 196–202.

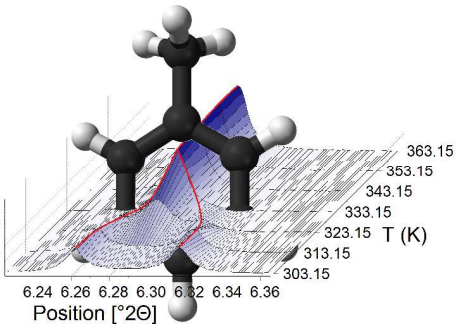

TOC Graphic (no label)

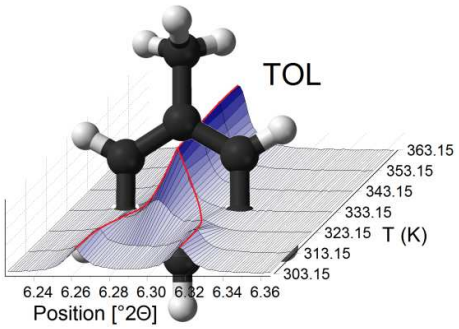
TOL
363.15
353.15
343.15
333.15
323.15
313.15
303.15
T (K)
6.24 6.26 6.28 6.30 6.32 6.34 6.36
Position [°2Θ]

TOC Graphic

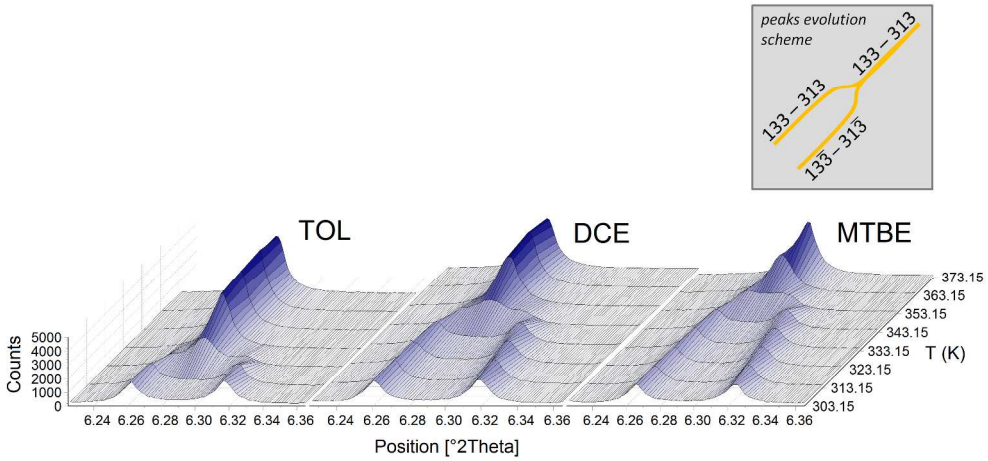

Figure 1. Cascade plot of TOL, DCE, and MTBE doped ZSM-5 samples in the 6.23–6.36 °2θ ranges within the 303–373 K temperature range.

935x450mm (96 x 96 DPI)

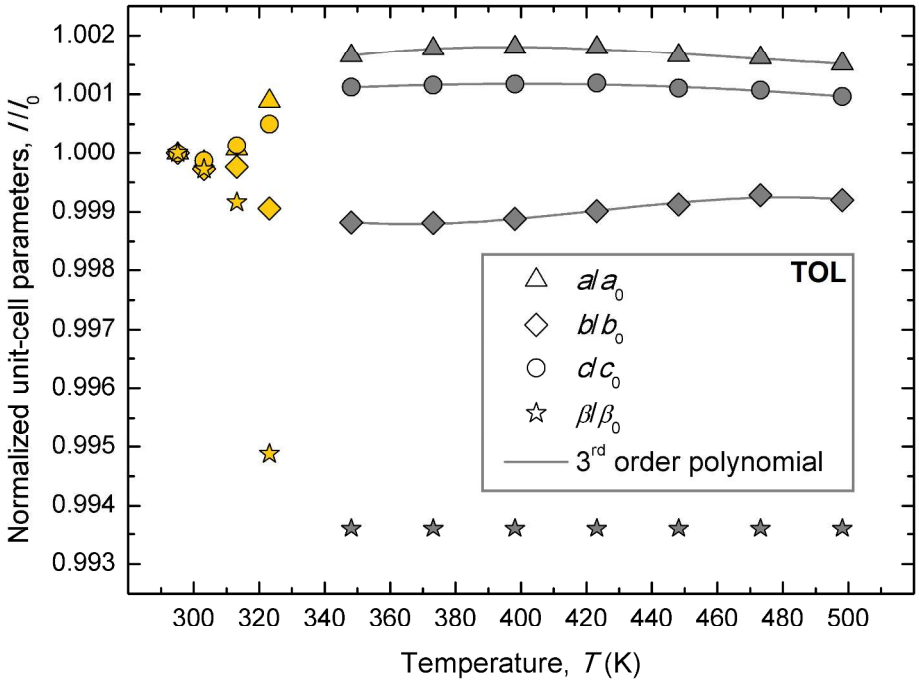

Figure 2 (A-F). Temperature dependence of lattice parameters (normalized unit-cell axes and β angle) obtained during heating cycles from room temperature to 498 K for the ZSM-5 zeolites with TOL (A), TOL-DCE (B), DCE (C), TOL-MTBE (D), DCE-MTBE (E), and MTBE (F), as adsorbed molecules. Yellow filled symbols refer to lattice parameters of the monoclinic structure, whereas gray filled symbols are those of the orthorhombic structure after the phase transition. Standard-deviation errors are within the symbol size. Solid lines through gray symbols are those fitted to a third-order polynomial equation.

796x609mm (96 x 96 DPI)

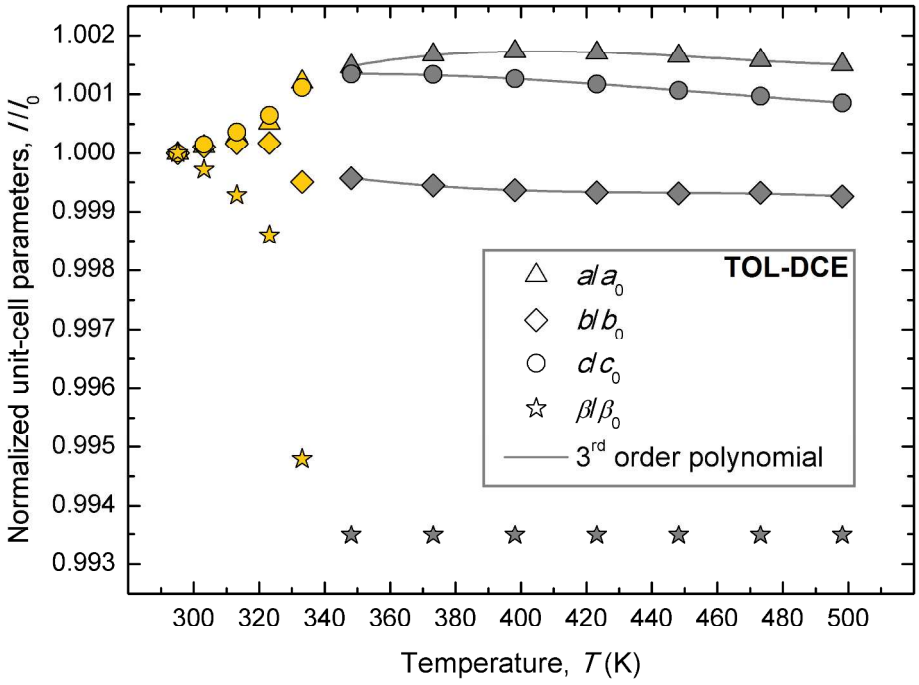

Figure 2 (A-F). Temperature dependence of lattice parameters (normalized unit-cell axes and β angle) obtained during heating cycles from room temperature to 498 K for the ZSM-5 zeolites with TOL (A), TOL-DCE (B), DCE (C), TOL-MTBE (D), DCE-MTBE (E), and MTBE (F), as adsorbed molecules. Yellow filled symbols refer to lattice parameters of the monoclinic structure, whereas gray filled symbols are those of the orthorhombic structure after the phase transition. Standard-deviation errors are within the symbol size. Solid lines through gray symbols are those fitted to a third-order polynomial equation.

796x609mm (96 x 96 DPI)

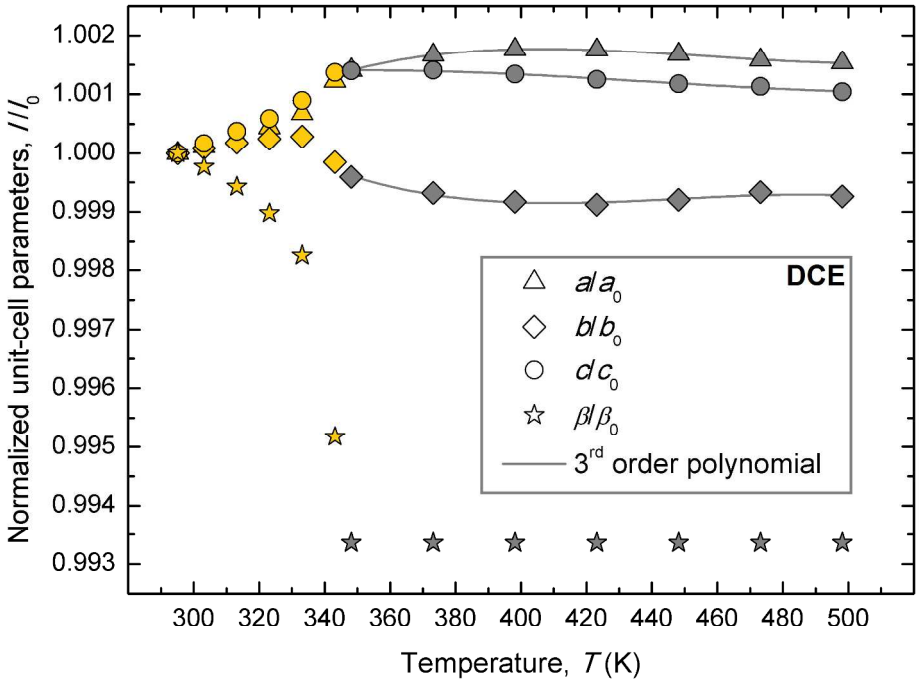

Figure 2 (A-F). Temperature dependence of lattice parameters (normalized unit-cell axes and β angle) obtained during heating cycles from room temperature to 498 K for the ZSM-5 zeolites with TOL (A), TOL-DCE (B), DCE (C), TOL-MTBE (D), DCE-MTBE (E), and MTBE (F), as adsorbed molecules. Yellow filled symbols refer to lattice parameters of the monoclinic structure, whereas gray filled symbols are those of the orthorhombic structure after the phase transition. Standard-deviation errors are within the symbol size. Solid lines through gray symbols are those fitted to a third-order polynomial equation.

796x609mm (96 x 96 DPI)

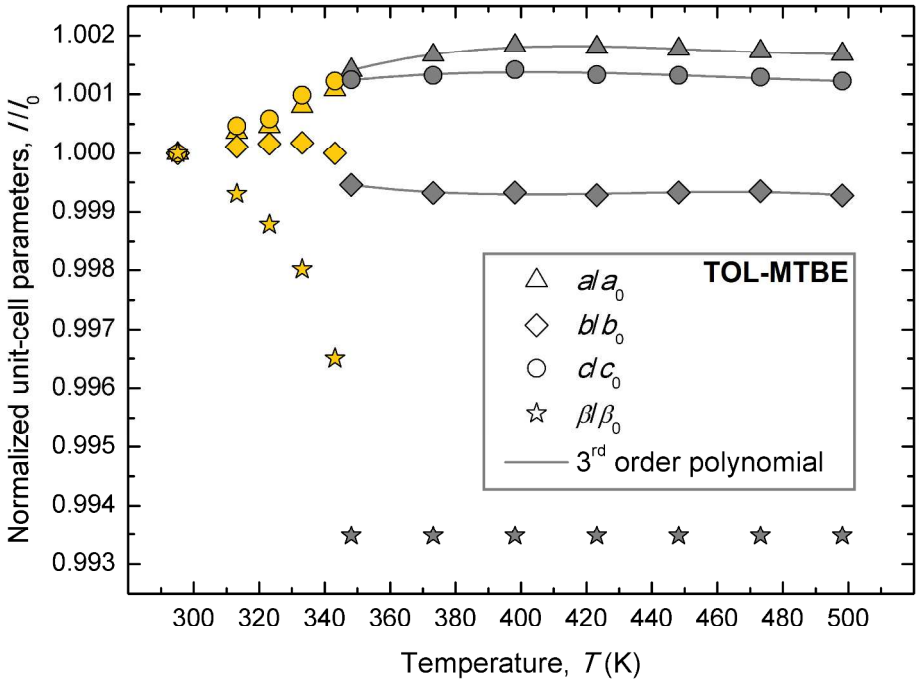

Figure 2 (A-F). Temperature dependence of lattice parameters (normalized unit-cell axes and β angle) obtained during heating cycles from room temperature to 498 K for the ZSM-5 zeolites with TOL (A), TOL-DCE (B), DCE (C), TOL-MTBE (D), DCE-MTBE (E), and MTBE (F), as adsorbed molecules. Yellow filled symbols refer to lattice parameters of the monoclinic structure, whereas gray filled symbols are those of the orthorhombic structure after the phase transition. Standard-deviation errors are within the symbol size. Solid lines through gray symbols are those fitted to a third-order polynomial equation.

796x609mm (96 x 96 DPI)

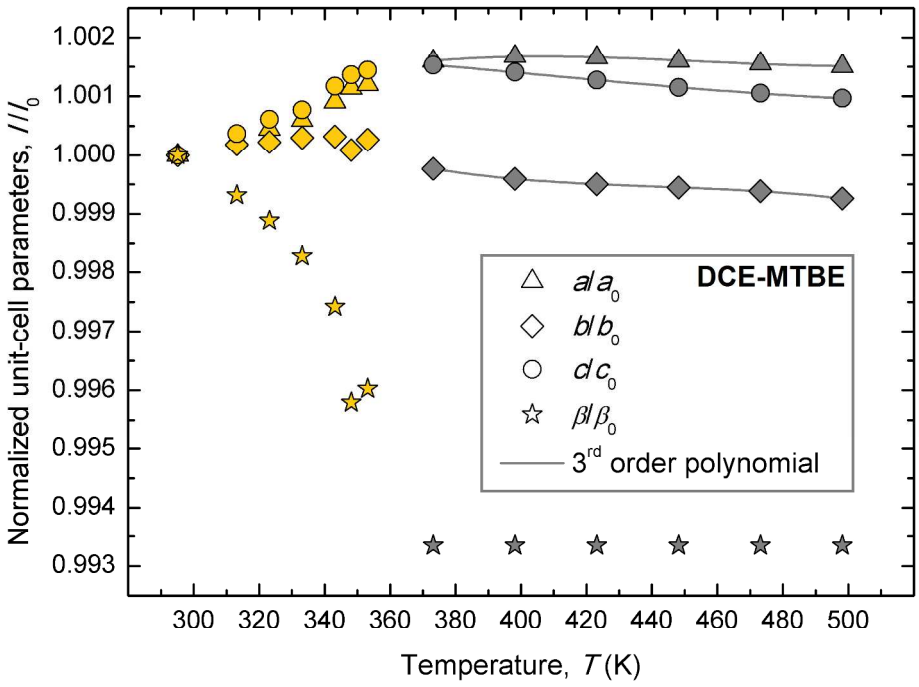

Figure 2 (A-F). Temperature dependence of lattice parameters (normalized unit-cell axes and β angle) obtained during heating cycles from room temperature to 498 K for the ZSM-5 zeolites with TOL (A), TOL-DCE (B), DCE (C), TOL-MTBE (D), DCE-MTBE (E), and MTBE (F), as adsorbed molecules. Yellow filled symbols refer to lattice parameters of the monoclinic structure, whereas gray filled symbols are those of the orthorhombic structure after the phase transition. Standard-deviation errors are within the symbol size. Solid lines through gray symbols are those fitted to a third-order polynomial equation.

796x609mm (96 x 96 DPI)

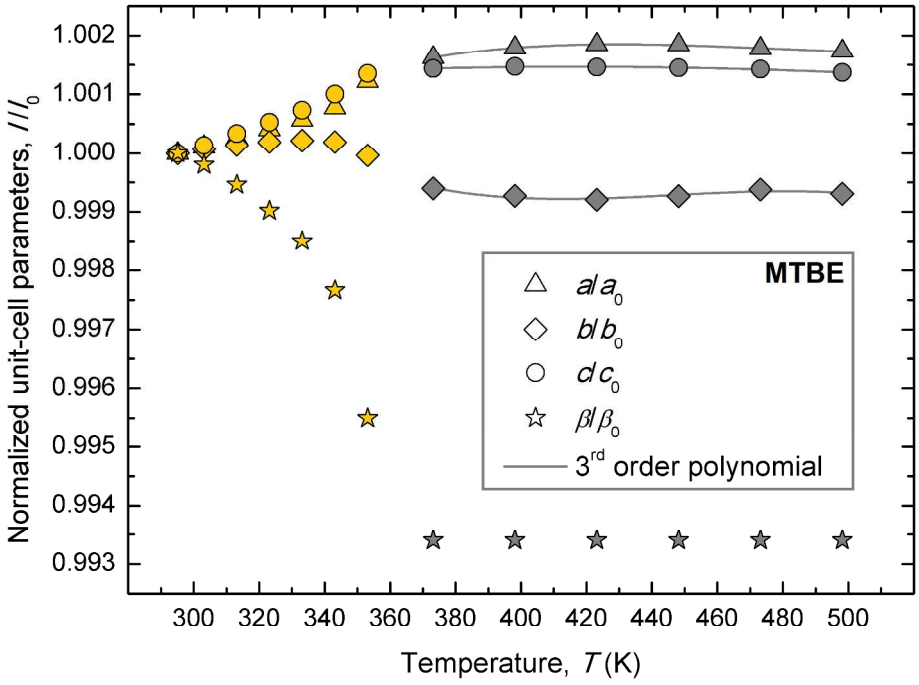

Figure 2 (A-F). Temperature dependence of lattice parameters (normalized unit-cell axes and β angle) obtained during heating cycles from room temperature to 498 K for the ZSM-5 zeolites with TOL (A), TOL-DCE (B), DCE (C), TOL-MTBE (D), DCE-MTBE (E), and MTBE (F), as adsorbed molecules. Yellow filled symbols refer to lattice parameters of the monoclinic structure, whereas gray filled symbols are those of the orthorhombic structure after the phase transition. Standard-deviation errors are within the symbol size. Solid lines through gray symbols are those fitted to a third-order polynomial equation.

796x609mm (96 x 96 DPI)

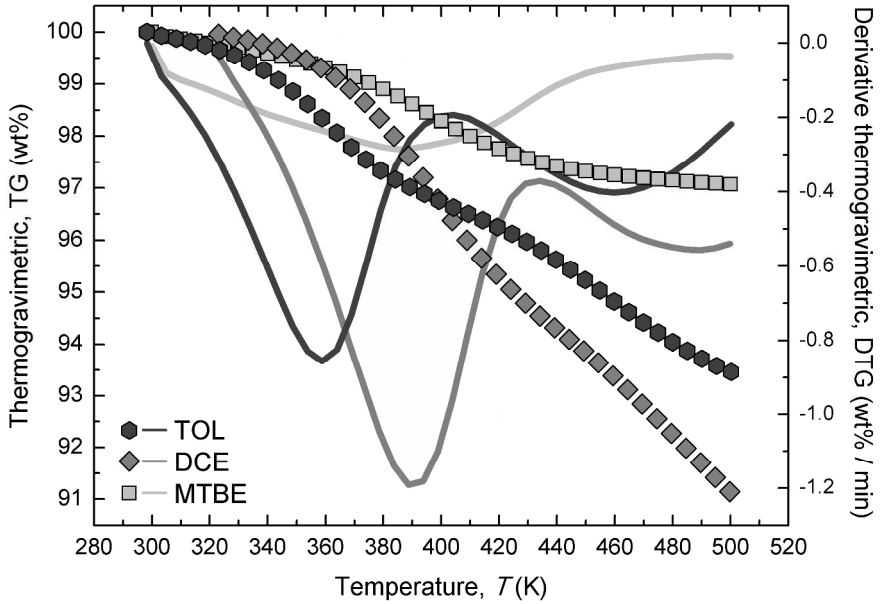

Figure 3 (A-B). Simultaneous thermogravimetric (TG; symbols) and derivative thermogravimetric (DTG; continuous lines) analyses of the investigated ZSM-5 samples with unary (A) and binary (B) adsorbed molecules in the temperature range 295−500 K.

531x370mm (144 x 144 DPI)

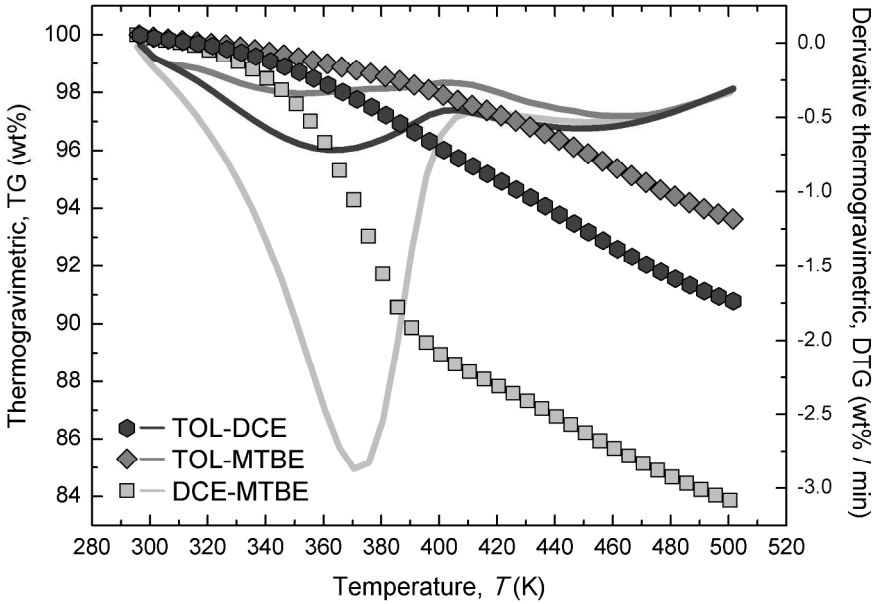

Figure 3 (A-B). Simultaneous thermogravimetric (TG; symbols) and derivative thermogravimetric (DTG; continuous lines) analyses of the investigated ZSM-5 samples with unary (A) and binary (B) adsorbed molecules in the temperature range 295−500 K.

531x370mm (144 x 144 DPI)

Figure 4 (A-L). Temperature dependence of spontaneous strain components and volume strain due to the m↔o phase transition in doped ZSM-5 structures (A, C, E, G, I, and K; cfr. Equations 1–4, and 6) coupled with the temperature dependence of the largest spontaneous strain tensor component e13, which behaves as the primary order parameter Q for each phase transition (B, D, F, H, J, and L; cfr. Equation 7).

254x194mm (300 x 300 DPI)

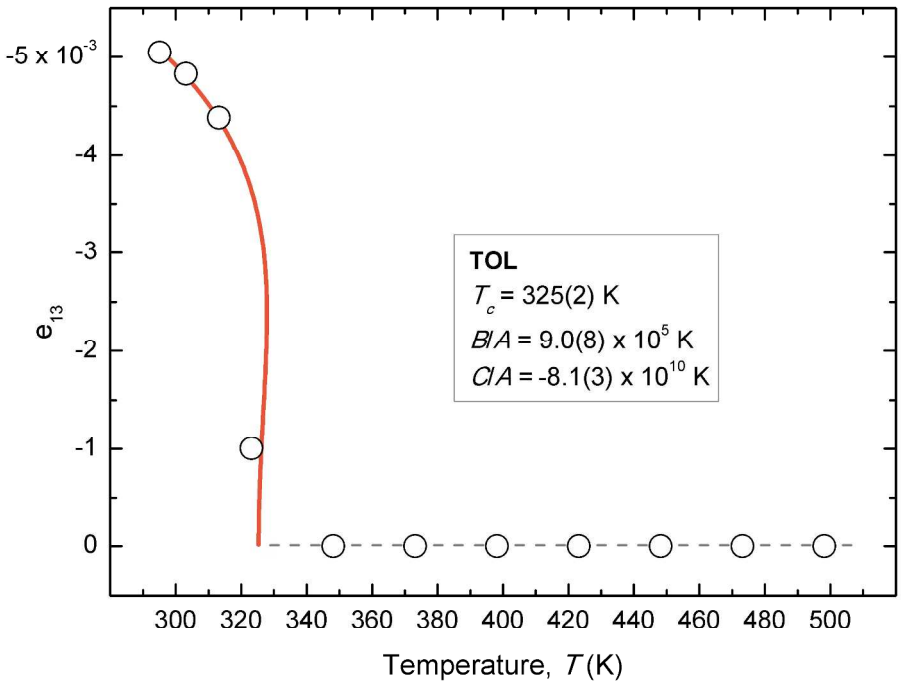

Figure 4 (A-L). Temperature dependence of spontaneous strain components and volume strain due to the m↔o phase transition in doped ZSM-5 structures (A, C, E, G, I, and K; cfr. Equations 1–4, and 6) coupled with the temperature dependence of the largest spontaneous strain tensor component e13, which behaves as the primary order parameter Q for each phase transition (B, D, F, H, J, and L; cfr. Equation 7).

531x406mm (144 x 144 DPI)

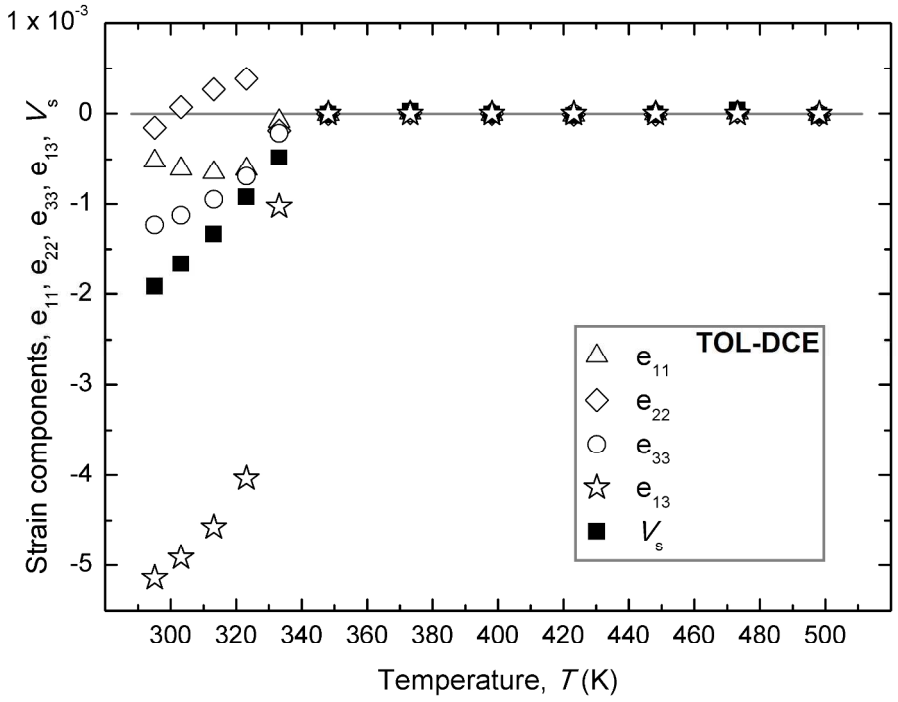

Figure 4 (A-L). Temperature dependence of spontaneous strain components and volume strain due to the m↔o phase transition in doped ZSM-5 structures (A, C, E, G, I, and K; cfr. Equations 1–4, and 6) coupled with the temperature dependence of the largest spontaneous strain tensor component e13, which behaves as the primary order parameter Q for each phase transition (B, D, F, H, J, and L; cfr. Equation 7).

531x406mm (144 x 144 DPI)

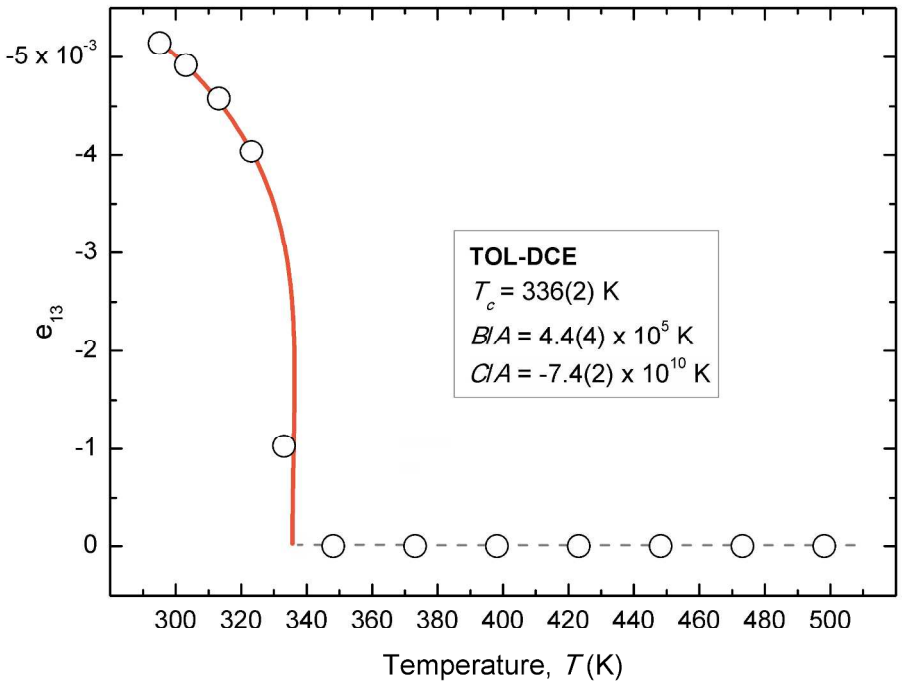

Figure 4 (A-L). Temperature dependence of spontaneous strain components and volume strain due to the m↔o phase transition in doped ZSM-5 structures (A, C, E, G, I, and K; cfr. Equations 1–4, and 6) coupled with the temperature dependence of the largest spontaneous strain tensor component e13, which behaves as the primary order parameter Q for each phase transition (B, D, F, H, J, and L; cfr. Equation 7).

531x406mm (144 x 144 DPI)

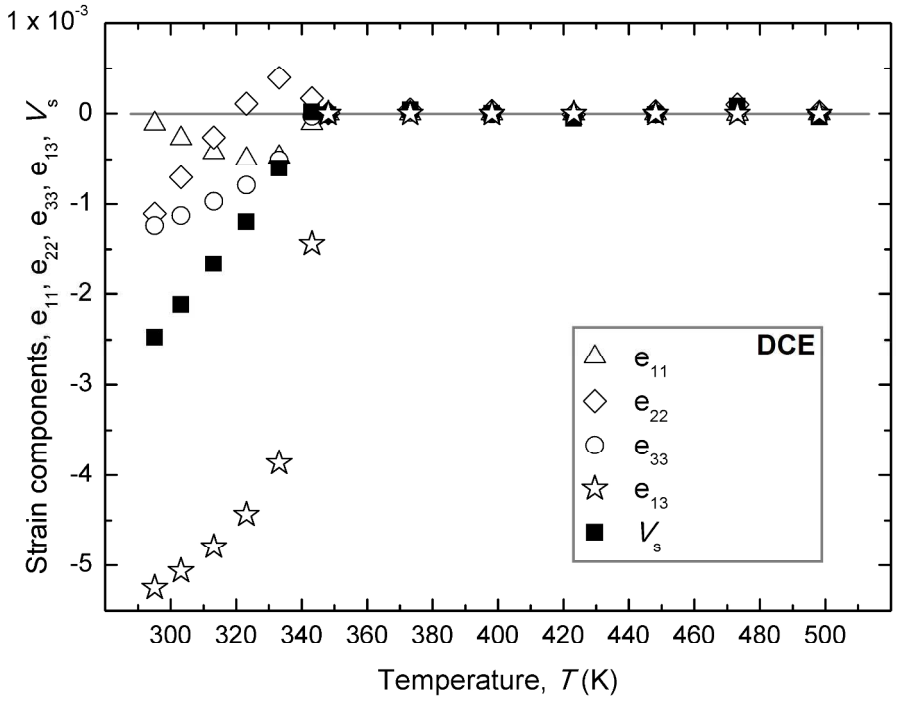

Figure 4 (A-L). Temperature dependence of spontaneous strain components and volume strain due to the m↔o phase transition in doped ZSM-5 structures (A, C, E, G, I, and K; cfr. Equations 1–4, and 6) coupled with the temperature dependence of the largest spontaneous strain tensor component e13, which behaves as the primary order parameter Q for each phase transition (B, D, F, H, J, and L; cfr. Equation 7).

531x406mm (144 x 144 DPI)

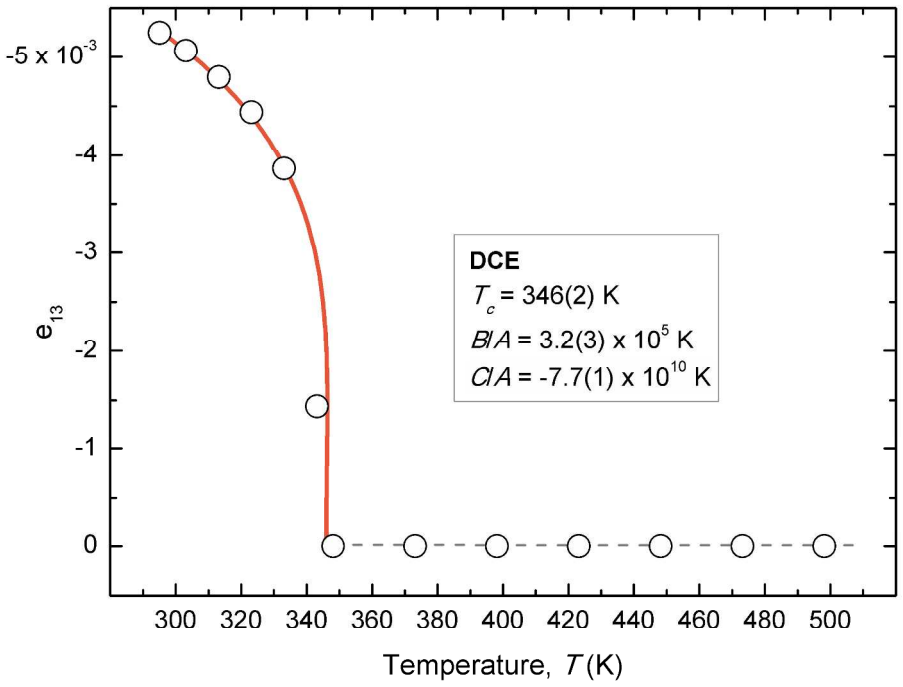

Figure 4 (A-L). Temperature dependence of spontaneous strain components and volume strain due to the m↔o phase transition in doped ZSM-5 structures (A, C, E, G, I, and K; cfr. Equations 1–4, and 6) coupled with the temperature dependence of the largest spontaneous strain tensor component e13, which behaves as the primary order parameter Q for each phase transition (B, D, F, H, J, and L; cfr. Equation 7).

531x406mm (144 x 144 DPI)

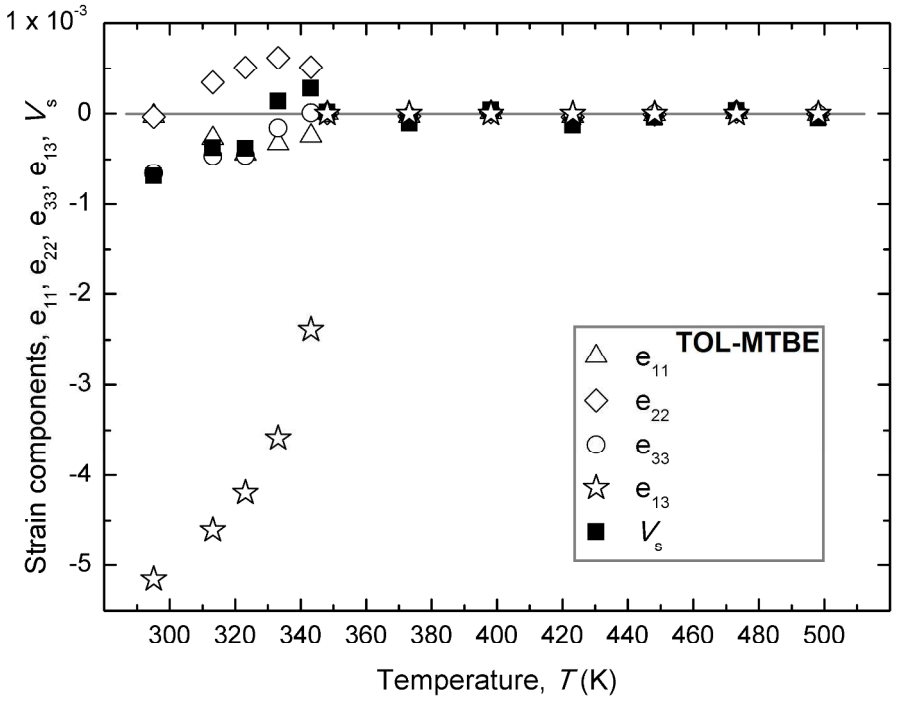

Figure 4 (A-L). Temperature dependence of spontaneous strain components and volume strain due to the m↔o phase transition in doped ZSM-5 structures (A, C, E, G, I, and K; cfr. Equations 1–4, and 6) coupled with the temperature dependence of the largest spontaneous strain tensor component e13, which behaves as the primary order parameter Q for each phase transition (B, D, F, H, J, and L; cfr. Equation 7).

531x406mm (144 x 144 DPI)

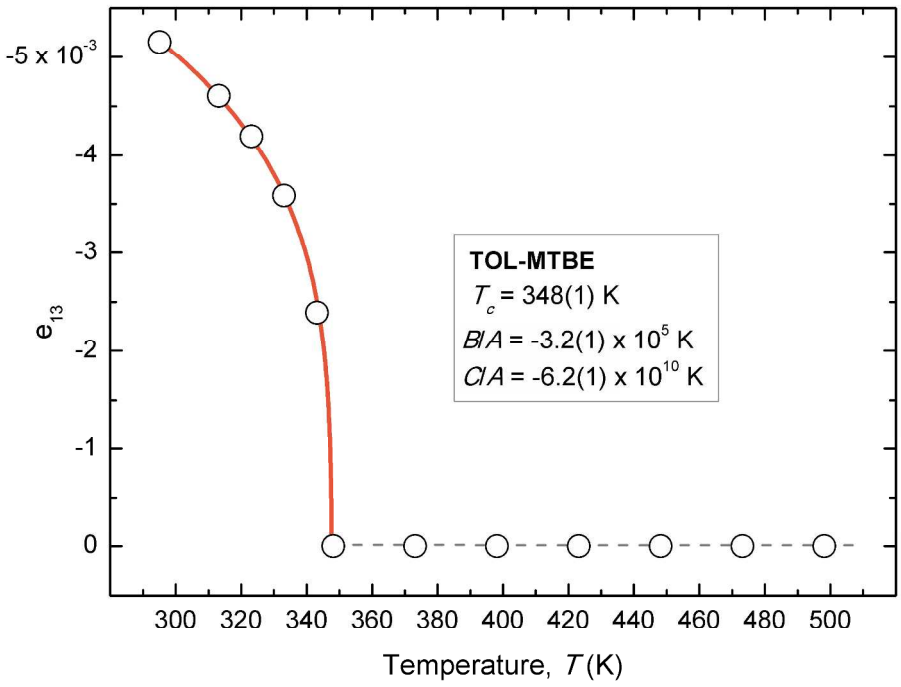

Figure 4 (A-L). Temperature dependence of spontaneous strain components and volume strain due to the m↔o phase transition in doped ZSM-5 structures (A, C, E, G, I, and K; cfr. Equations 1–4, and 6) coupled with the temperature dependence of the largest spontaneous strain tensor component e13, which behaves as the primary order parameter Q for each phase transition (B, D, F, H, J, and L; cfr. Equation 7).

531x406mm (144 x 144 DPI)

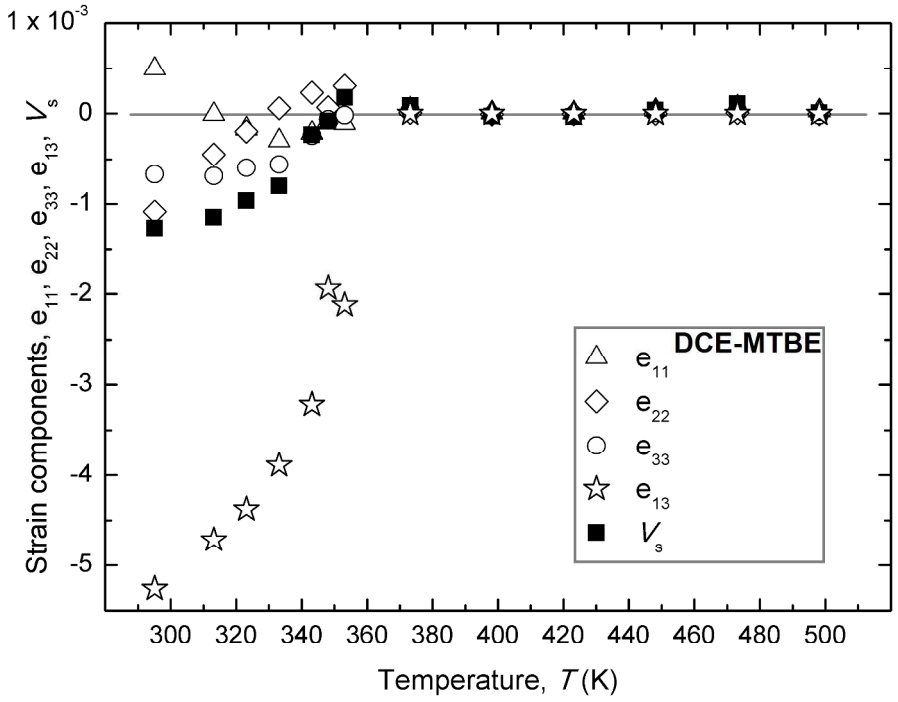

Figure 4 (A-L). Temperature dependence of spontaneous strain components and volume strain due to the m↔o phase transition in doped ZSM-5 structures (A, C, E, G, I, and K; cfr. Equations 1–4, and 6) coupled with the temperature dependence of the largest spontaneous strain tensor component e13, which behaves as the primary order parameter Q for each phase transition (B, D, F, H, J, and L; cfr. Equation 7).

531x406mm (144 x 144 DPI)

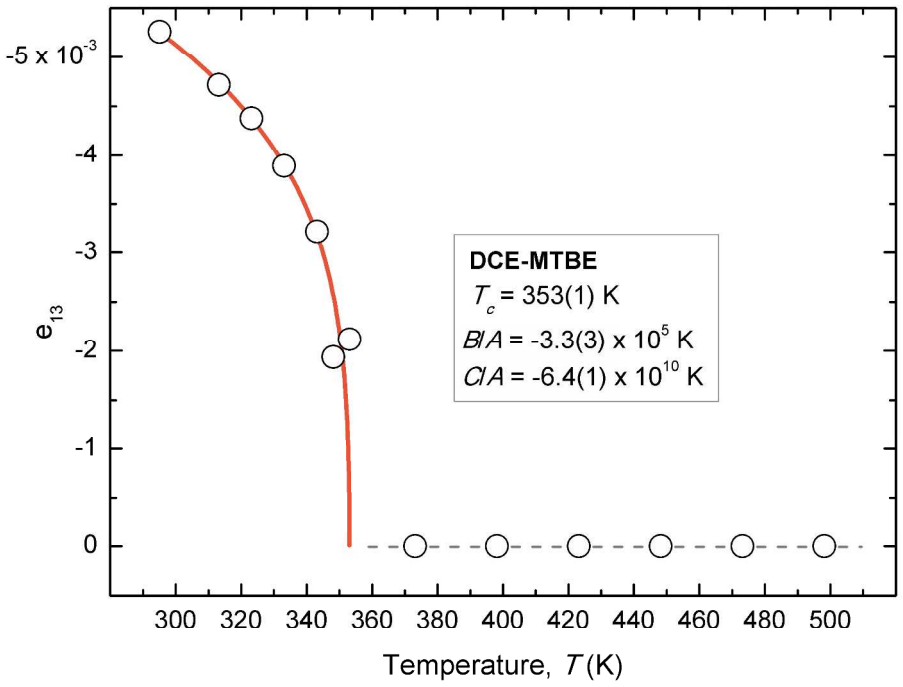

Figure 4 (A-L). Temperature dependence of spontaneous strain components and volume strain due to the m↔o phase transition in doped ZSM-5 structures (A, C, E, G, I, and K; cfr. Equations 1–4, and 6) coupled with the temperature dependence of the largest spontaneous strain tensor component e13, which behaves as the primary order parameter Q for each phase transition (B, D, F, H, J, and L; cfr. Equation 7).

531x406mm (144 x 144 DPI)

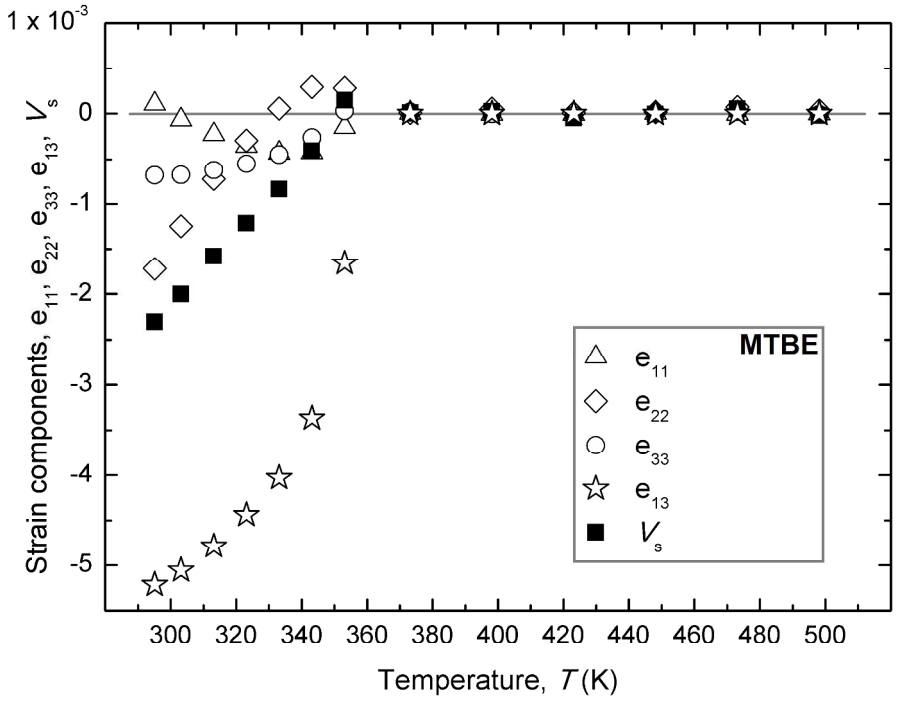

Figure 4 (A-L). Temperature dependence of spontaneous strain components and volume strain due to the m↔o phase transition in doped ZSM-5 structures (A, C, E, G, I, and K; cfr. Equations 1–4, and 6) coupled with the temperature dependence of the largest spontaneous strain tensor component e13, which behaves as the primary order parameter Q for each phase transition (B, D, F, H, J, and L; cfr. Equation 7).

531x406mm (144 x 144 DPI)

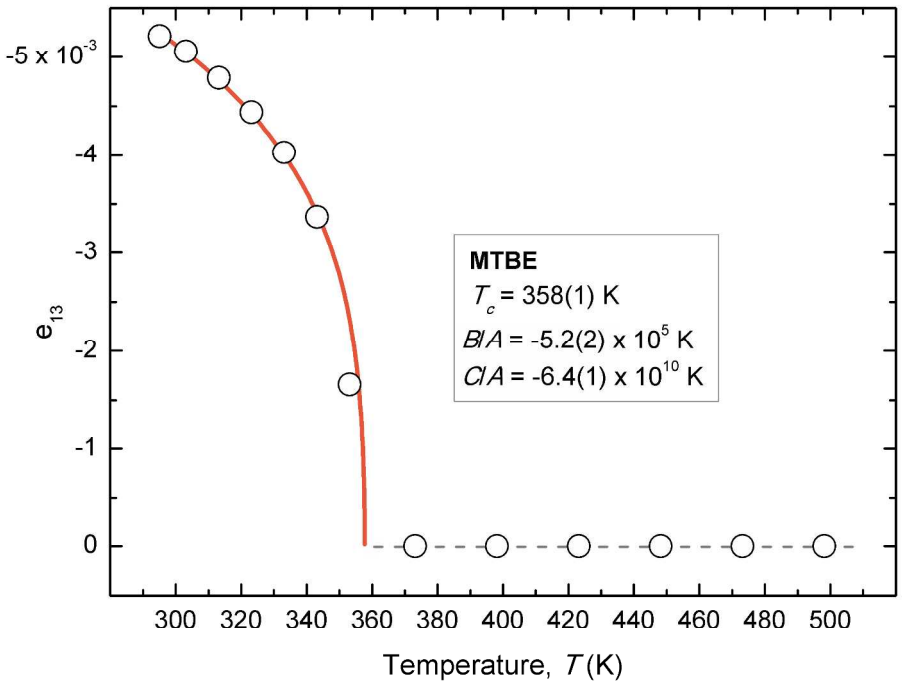

Figure 4 (A-L). Temperature dependence of spontaneous strain components and volume strain due to the m↔o phase transition in doped ZSM-5 structures (A, C, E, G, I, and K; cfr. Equations 1–4, and 6) coupled with the temperature dependence of the largest spontaneous strain tensor component e13, which behaves as the primary order parameter Q for each phase transition (B, D, F, H, J, and L; cfr. Equation 7).

531x406mm (144 x 144 DPI)

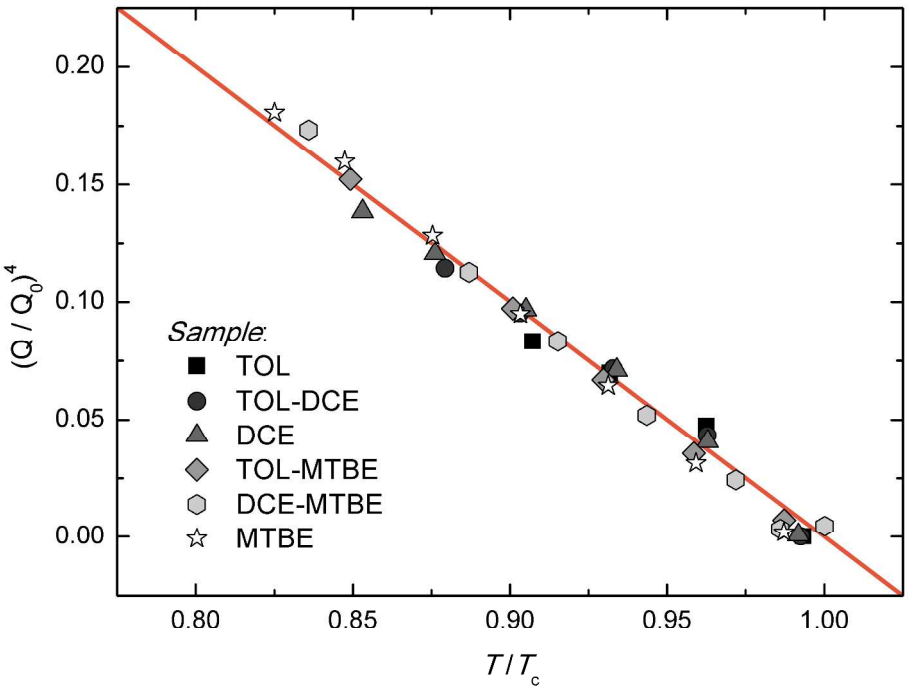

Figure 5 (A-B). (A) Normalized order parameter, (Q / Q0)4, and (B) normalized monoclinic angles, (β / β0), as a function of the normalized transformation temperature (T / Tc, for T < Tc).

796x609mm (96 x 96 DPI)

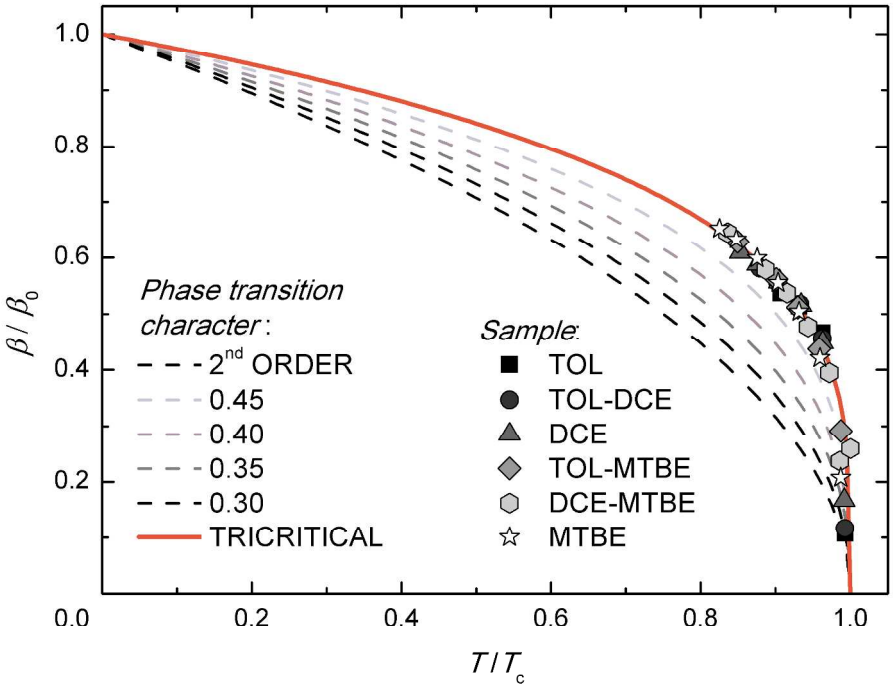

Figure 5 (A-B). (A) Normalized order parameter, (Q / Q0)4, and (B) normalized monoclinic angles, (β / β0), as a function of the normalized transformation temperature (T / Tc, for T < Tc).

254x194mm (300 x 300 DPI)

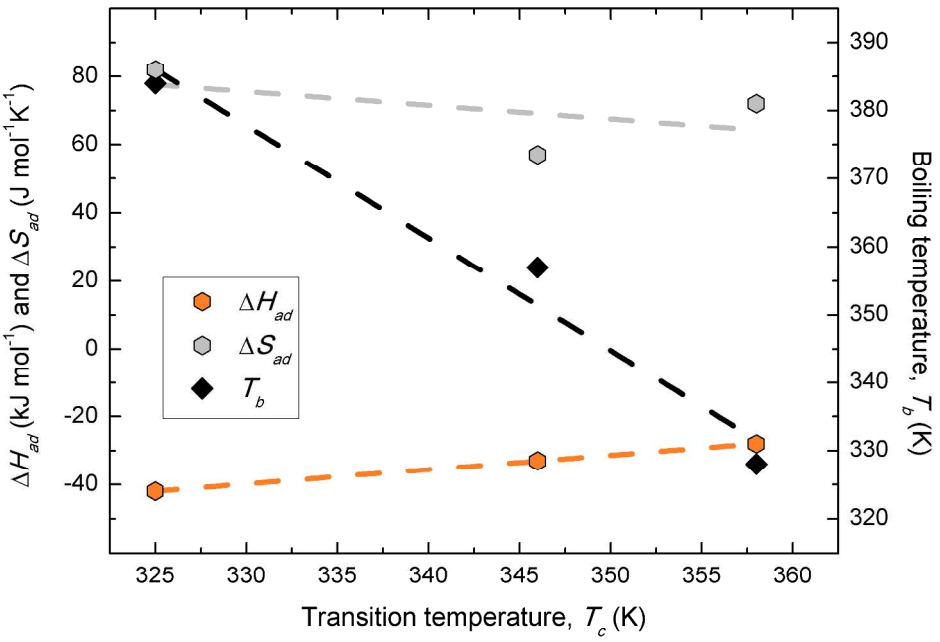

Figure 6. Boiling point temperature (Tb), enthalpy (ΔHad) and entropy (ΔSad) of the adsorption of TOL, DCE, and MTBE from aqueous solution as a function of the transition temperature (Tc).

796x564mm (96 x 96 DPI)

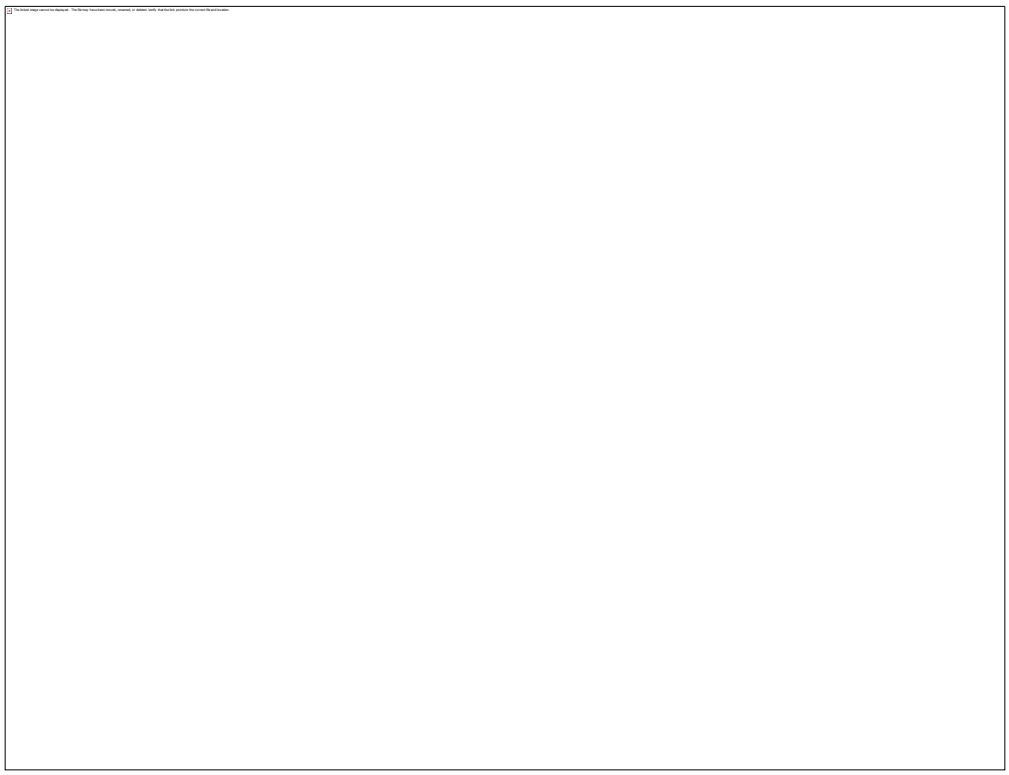

Figure 7 (A-B). (A) Monoclinic-orthorhombic m↔o phase transition temperature (Tc), and (B) enthalpy (ΔHad) of the adsorption of organic contaminants for the ZSM-5 investigated vs calculated ratio of the C/A Landau coefficients (cfr. Equation 7). Empty symbols in B refer to ΔHad data extrapolated from equation 11.

796x609mm (96 x 96 DPI)

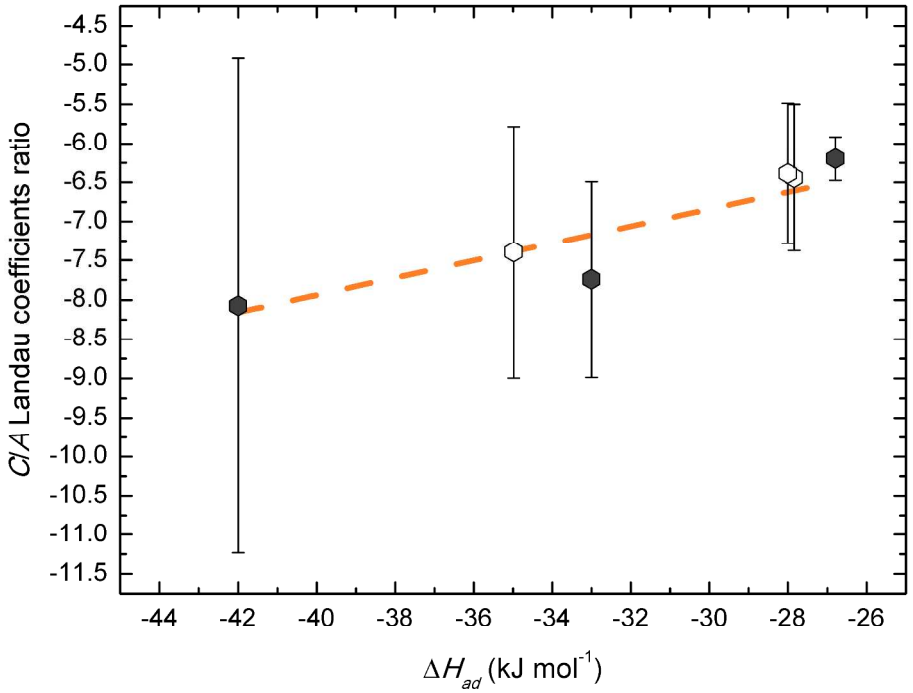

Figure 7 (A-B). (A) Monoclinic-orthorhombic m↔o phase transition temperature (Tc), and (B) enthalpy (ΔHad) of the adsorption of organic contaminants for the ZSM-5 investigated vs calculated ratio of the C/A Landau coefficients (cfr. Equation 7). Empty symbols in B refer to ΔHad data extrapolated from equation 11.

796x609mm (96 x 96 DPI)

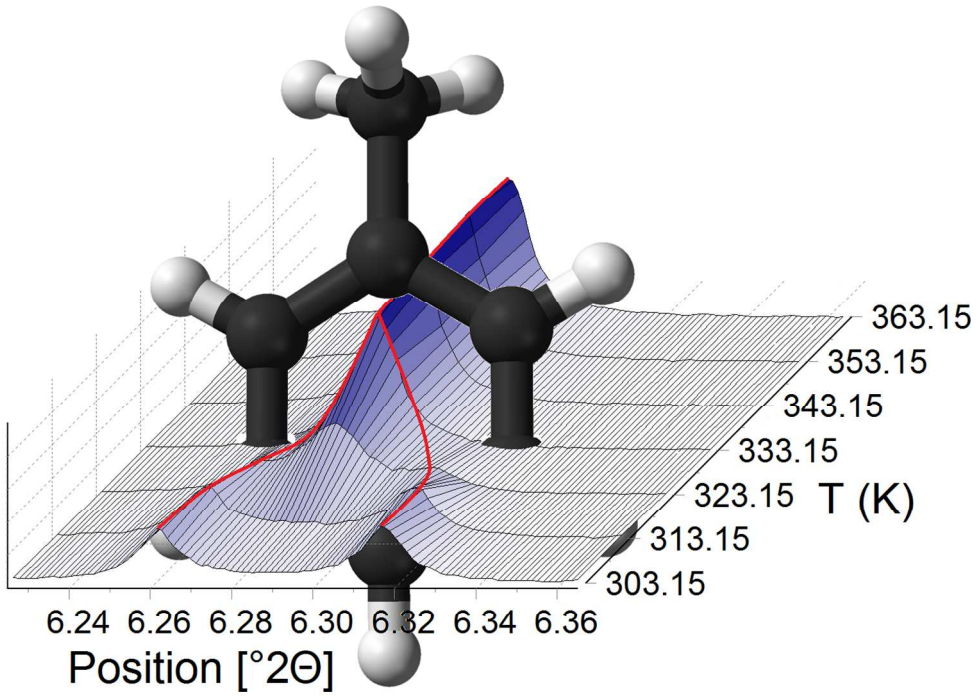

TOC Graphic (no label)

389x282mm (96 x 96 DPI)

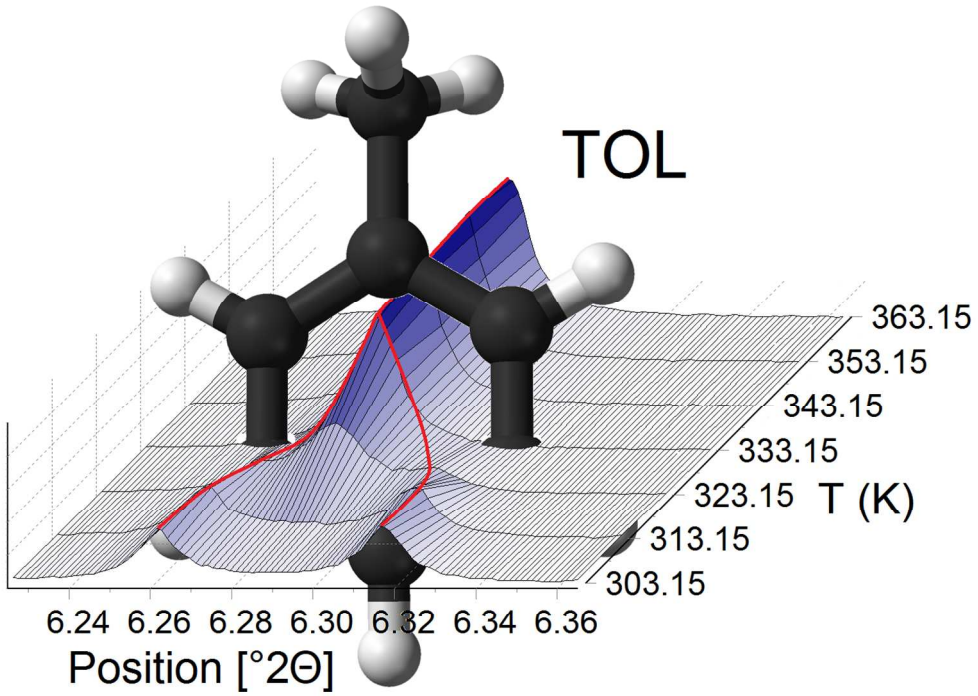

TOC Graphic

389x282mm (96 x 96 DPI)